JOURNAL OF GEOPHYSICAL RESEARCH, VOL. 114, D12305, doi:10.1029/2008JD011420, 2009

Impact of geoengineered aerosols on the troposphere and stratosphere

Simone Tilmes,[1] Rolando R. Garcia,[1] Douglas E. Kinnison,[1] Andrew Gettelman,[1] and Philip J. Rasch[2]

Received 5 November 2008; revised 10 March 2009; accepted 15 April 2009; published 27 June 2009.

[1] A coupled chemistry climate model, the Whole Atmosphere Community Climate Model was used to perform a transient climate simulation to quantify the impact of geoengineered aerosols on atmospheric processes. In contrast to previous model studies, the impact on stratospheric chemistry, including heterogeneous chemistry in the polar regions, is considered in this simulation. In the geoengineering simulation, a constant stratospheric distribution of volcanic-sized, liquid sulfate aerosols is imposed in the period 2020–2050, corresponding to an injection of 2 Tg S/a. The aerosol cools the troposphere compared to a baseline simulation. Assuming an Intergovernmental Panel on Climate Change A1B emission scenario, global warming is delayed by about 40 years in the troposphere with respect to the baseline scenario. Large local changes of precipitation and temperatures may occur as a result of geoengineering. Comparison with simulations carried out with the Community Atmosphere Model indicates the importance of stratospheric processes for estimating the impact of stratospheric aerosols on the Earth's climate. Changes in stratospheric dynamics and chemistry, especially faster heterogeneous reactions, reduce the recovery of the ozone layer in middle and high latitudes for the Southern Hemisphere. In the geoengineering case, the recovery of the Antarctic ozone hole is delayed by about 30 years on the basis of this model simulation. For the Northern Hemisphere, a onefold to twofold increase of the chemical ozone depletion occurs owing to a simulated stronger polar vortex and colder temperatures compared to the baseline simulation, in agreement with observational estimates.

Citation: Tilmes, S., R. R. Garcia, D. E. Kinnison, A. Gettelman, and P. J. Rasch (2009), Impact of geoengineered aerosols on the troposphere and stratosphere, *J. Geophys. Res.*, *114*, D12305, doi:10.1029/2008JD011420.

1. Introduction

[2] The impact of increasing greenhouse gases on the atmosphere was assessed by the *Intergovernmental Panel on Climate Change* (*IPCC*) [2007]. This report discussed the extent of possible climate change depending on different CO_2 emission scenarios, and the impact of these changes on the environment. Thus far, there is no general agreement whether the response by the world's nations to reduce greenhouse gas emissions will be sufficient to restrict global warming to tolerable levels. Rapidly increasing surface temperatures, especially in the polar regions may result, in addition to many other possible consequences, in faster-than-expected melting of the Greenland ice sheet and, therefore, a drastic increase of sea level, a serious danger for coastal regions.

[3] Recent studies have advocated the search for "novel options" that could cool the troposphere and counteract global warming. In particular, *Crutzen* [2006] and *Cicerone* [2006] have encouraged scientists to study such options and to quantify their effects, including undesirable side effects, and to critically question the suggested approaches. One approach to cool the atmosphere and therefore delay drastic impacts of global warming is the injection of sulfur into the stratosphere [e.g., *Budyko*, 1977; *Crutzen*, 2006]. The resulting enhanced layer of sulfate aerosols in the stratosphere is expected to increase the albedo of the planet. Examples of a natural injection of large amounts of sulfur into the stratosphere have been provided by recent large volcanic eruptions, such as those of El Chichón and Mount Pinatubo. These provide observational evidence of the impact of enhanced sulfate aerosols on climate [*Robock*, 2000; *Stenchikov et al.*, 2002]. Model simulations have also been performed to quantify the effect of geoengineered aerosols on the climate system [*Wigley*, 2006; *Rasch et al.*, 2008b; *Robock et al.*, 2008]. Depending on how much sulfur is injected, tropospheric temperatures could be reduced effectively under present and future CO_2 conditions.

[4] Previous atmospheric model simulations did not include stratospheric dynamics and chemical processes in any detail to analyze the impact of geoengineering. *Solomon et al.* [1996] have shown that enhanced stratospheric aerosol

[1]Atmospheric Chemistry Division, National Center of Atmospheric Research, Boulder, Colorado, USA.
[2]Pacific Northwest National Laboratory, Richland, Washington, USA.

0148-0227/09/2008JD011420$09.00

levels after a volcanic eruption, would disturb ozone photochemistry in midlatitudes, because of the suppression of stratospheric NO_x, leading to enhanced halogen catalyzed ozone depletion. A study by *Tilmes et al.* [2008], based on an empirical projection of past ozone loss in the polar vortex to future conditions, estimated a significant increase of stratospheric ozone depletion in high polar latitudes. A substantial decrease of the ozone layer significantly increases dangerous UV radiation at the Earth's surface and harmful impacts on the biosphere [e.g., *United Nations Environment Programme and Environmental Effects Assessment Panel*, 2005]. However, the results of *Tilmes et al.* [2008] do not take into account possible changes in stratospheric dynamics as a result of the application of geoengineered aerosols. Changes in stratospheric ozone produce changes in temperature and dynamics, which can in turn influence the tropospheric climate [*Sassi et al.*, 2005; *Thompson et al.*, 2005; *Perlwitz et al.*, 2008].

[5] Here, we use the Whole Atmosphere Community Climate Model, Version 3 (WACCM3), to explore the impact of geoengineered aerosols on tropospheric climate, as well as on stratospheric chemistry and dynamics. The model, and its ability to produce reliable results under enhanced stratospheric aerosol conditions, is discussed in section 2.1. In section 2.2, we describe in detail the setup of our near future model simulation, between 2010 and 2050. In general, a baseline simulation with background aerosols is compared to a "geoengineering" simulation in which a fixed amount of sulfur aerosols is added into the stratosphere. Both simulations include projected greenhouse gas and halogen species changes. The assumed amount of sulfur added to form volcanic-sized aerosols was estimated in an earlier study by *Rasch et al.* [2008b] to approximately counteract surface temperature changes around 2050 due to greenhouse gas increases.

[6] The climate impact of geoengineered aerosols is discussed for different regions of the atmosphere. Global changes of temperatures between present and future, and between the two simulations performed, are discussed in section 3. Section 4 describes the impact of this specific geoengineering approach at the Earth's surface, with a focus on temperatures, sea-ice content and precipitation. We further compare WACCM3 surface temperature changes to results from a previously performed geoengineering simulation that used the Community Atmosphere Model (CAM) [*Rasch et al.*, 2008b]. In section 5, we discuss the impact of geoengineering on stratospheric chemistry and dynamics, and the importance of ozone production, loss rates, and advection on the ozone column, under the influence of geoengineered aerosols in the future climate (between 2040 and 2050). In section 6, we examine the impact of sulfate aerosols on polar vortex dynamics and resulting changes in heterogeneous chemistry on polar chemical ozone depletion. Finally, in section 7, we summarize the impact of sulfate aerosols on the climate system.

2. Model and Simulation

2.1. Model Description

[7] WACCM3 is a fully interactive chemistry-climate model with 66 vertical levels from the ground to 4.5×10^{-6} hPa ($\approx$150 km geometric altitude). The vertical resolution of WACCM3 in the lower stratosphere below 30 km is 1.1–1.4 km. The horizontal resolution used in this study is 1.9° latitude $\times$2.5° longitude. The initialization and parameterization of the model is summarized by *Garcia et al.* [2007], on the basis of earlier WACCM3 model simulations. These earlier simulations were carried out as part of the CCM Validation (CCMVal) activity of SPARC (Stratospheric Processes and their Role in Climate) [*Eyring et al.*, 2005, 2006] and were used for model intercomparison [*Eyring et al.*, 2006]. An ensemble simulation of three realizations of the period 1950–2003 denoted as reference simulation one (REF1) was performed, as well as three realizations of the period between 2000 and 2050 denoted as reference simulation two, or REF2.

[8] The chemical module of WACCM3 is based upon the 3-D chemical transport Model of OZone and Related Tracers, Version 3 (MOZART3). A detailed description of MOZART3, i.e., the gas-phase and heterogeneous processes, is given by *Kinnison et al.* [2007]. In this model, heterogeneous processes take place on liquid sulfate aerosols and solid aerosols [*Considine et al.*, 2000]. The aerosol distribution is derived using a prescribed surface area density (SAD) field [*Thomason et al.*, 1997; *Thomason and Peter*, 2006]. Further details about the representation of stratospheric aerosols are given by *Kinnison et al.* [2007, auxiliary material A1.4]. An evaluation of polar stratospheric processes in the WACCM3 REF1 simulation using the same chemical scheme is given by *Tilmes et al.* [2007].

[9] In contrast to earlier simulations, the atmospheric general circulation model is coupled to a slab ocean model with a simple sea ice model controlled only by heat and moisture fluxes. In this way, the heat exchange between ocean and atmosphere is considered. The prescribed ocean heat fluxes were derived for the simulation period using the Community Climate System Model Version 3 (CCSM3) [*Collins et al.*, 2006], based on the IPCC A1B greenhouse gas scenario. A slab ocean model does not respond to possible circulation changes as a result of environmental changes, in contrast to a full deep-ocean model. Therefore, our simulation might underestimate the influence of the ocean temperature response.

[10] In addition to a slab ocean model, we introduced a stratospheric aerosol heating term in the simulation. The aerosol heating is a function of a prescribed aerosol distribution varying in space and time that has a size distribution similar to that seen after a volcanic eruption. The mass distribution is calculated from the prescribed surface area density (SAD) assuming a log-normal size distribution. It is then passed (along with all the other radiatively active gases and aerosols) to the radiative transfer code, which in turn calculates heating and cooling rates used in the integration.

[11] To calibrate the model response we have made one simulation for the years between 1984 and 2003 (labeled REF1.3v) in which the aerosol distribution is prescribed using the time and space distribution retrieved from SAGE II as described by *Thomason et al.* [1997]. This simulation is identical to one of the REF1 realizations (REF1.3) using the same horizontal and vertical resolution, but additionally including the aerosol heating.

[12] The temperature difference between REF1.3v, including the aerosol heating and REF1.3, without the aerosol heating, can be directly ascribed as the impact of volcanic

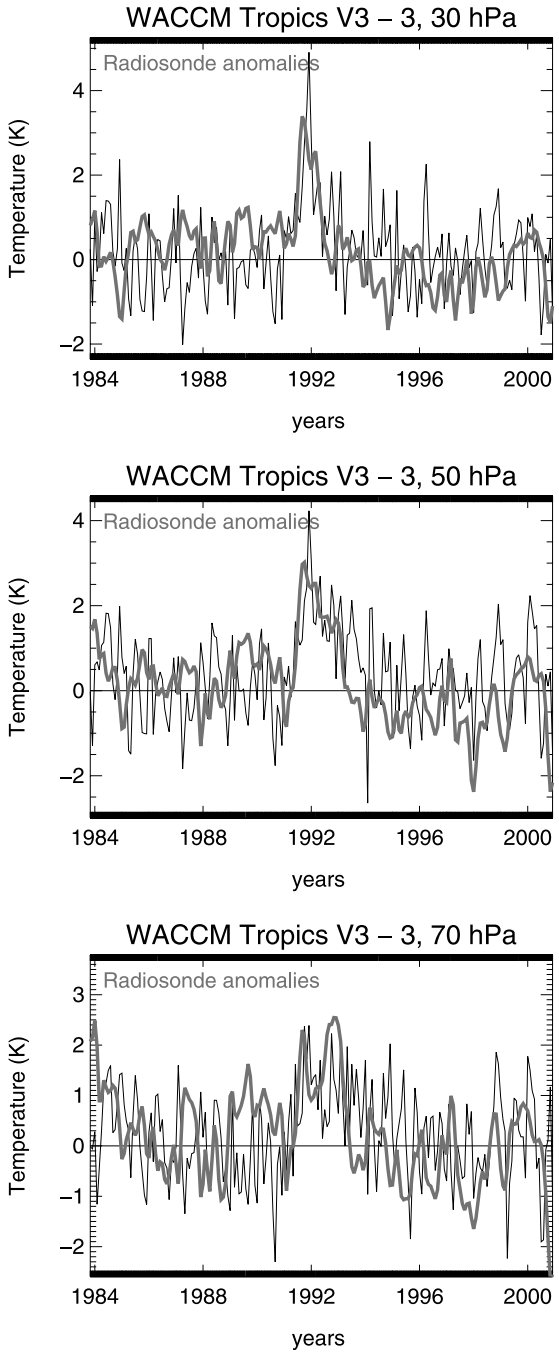

Figure 1. Temperature difference between the REF1.3v and REF1.3 simulations (see text for details) for different pressure levels (black lines). Temperature anomalies from radiosonde observations [*Randel et al.*, 2009] are shown as grey lines.

aerosols. In Figure 1, temperature differences between the two model runs, using monthly and zonal averages in the tropics (between 30° and 30°S), are compared to radiosonde temperature anomalies for the period 1984–2000 [*Randel et al.*, 2009]. The monthly averaged anomalies of observations are based on 14 tropical radiosonde stations.

[13] The eruption of Mount Pinatubo in 1991 injected large amounts of sulfur into the stratosphere. Significant temperature increases of about 1–3 K between 70 and 30 hPa occurred after 1991 for both the differences in the simulations (black line) and radiosonde anomalies (grey line) (Figure 1). For all three pressure levels, temperature anomalies agree well between model and observations. Therefore, we expect a reliable response of the aerosol heating in the model run when using geoengineered volcanic-sized aerosols.

2.2. Setup of the Future Control and Geoengineering Model Runs

[14] We performed two simulations to analyze the impact of geoengineered aerosols on the tropospheric and stratospheric dynamics, and stratospheric chemistry. The control, or "baseline" model run, is initialized as a REF2 model run, following the CCMVal definition [*Eyring et al.*, 2006], and covers the period between 2010 and 2050. Increasing greenhouse gases, based on the IPCC A1B scenario [*IPCC*, 2007], are included in this simulation, as well as changes in anthropogenic halogen emissions. Initialized SAD and the resulting H_2SO_4 mass in the model are prescribed using a climatology for a nonvolcanic period from SAGE II [*Thomason et al.*, 1997].

[15] The geoengineering model run is set up identically to the baseline run between 2010 and 2020. However, starting in the year 2020, the SAD is increased from background to an enhanced, fixed SAD distribution. This SAD is calculated from the SO_4 distribution derived in the study of *Rasch et al.* [2008b]. *Rasch et al.* [2008b] used the NCAR CAM model to derive aerosol distributions for different scenarios, with varying amounts of sulfur injection in the tropics, two different-sized aerosol types, and two different CO_2 conditions. Here, we use the "volc2" case of *Rasch et al.* [2008b], where 2 Tg S/a of volcanic aerosols are injected into a present-day CO_2 environment. "Volcanic like" aerosols are assumed to have a dry mode radius of 0.37 μm and a standard deviation of 1.25 μm, which corresponds to an effective radius of about 0.43 μm.

[16] The monodisperse particle distribution assumed here is an approximation that does not cover the entire particle size spectrum in the atmosphere. Further, the initial coagulation time of sulfate aerosols depends on the injection scheme (initial aerosol size) and the number density of aerosols already in the stratosphere. As discussed in detail by *Rasch et al.* [2008b, section 2c and references therein], a distribution dominated by background-sized particles, as considered in earlier studies [e.g., *Rasch et al.*, 2008b; *Tilmes et al.*, 2008], is not likely to be maintained given the amount of aerosols needed to cool the Earth's climate. Microphysical studies have shown that, under background conditions, newly injected aerosol particles reach stabilized sizes larger than 0.3 μm in $\approx$50 days after a volcanic eruption [*Zhao et al.*, 1995], and also in the case of geoengineering (M. Mills, personal communication, 2008). Effective radii under stabilized conditions were calculated between 0.3 and 0.5 μm, which is consistent with our assumption and with observations taken after the eruption of Mount Pinatubo [*Russell et al.*, 1996]. In the case of an enhanced aerosol burden, newly injected aerosol particles coagulate and grow toward volcanic-sized particles in a much shorter time [e.g., *Seinfeld and Pandis*, 1998; *Mills*, 1996; *Turco et al.*, 1979]. To evaluate the impact of the entire size spectrum of geoengineered stratospheric

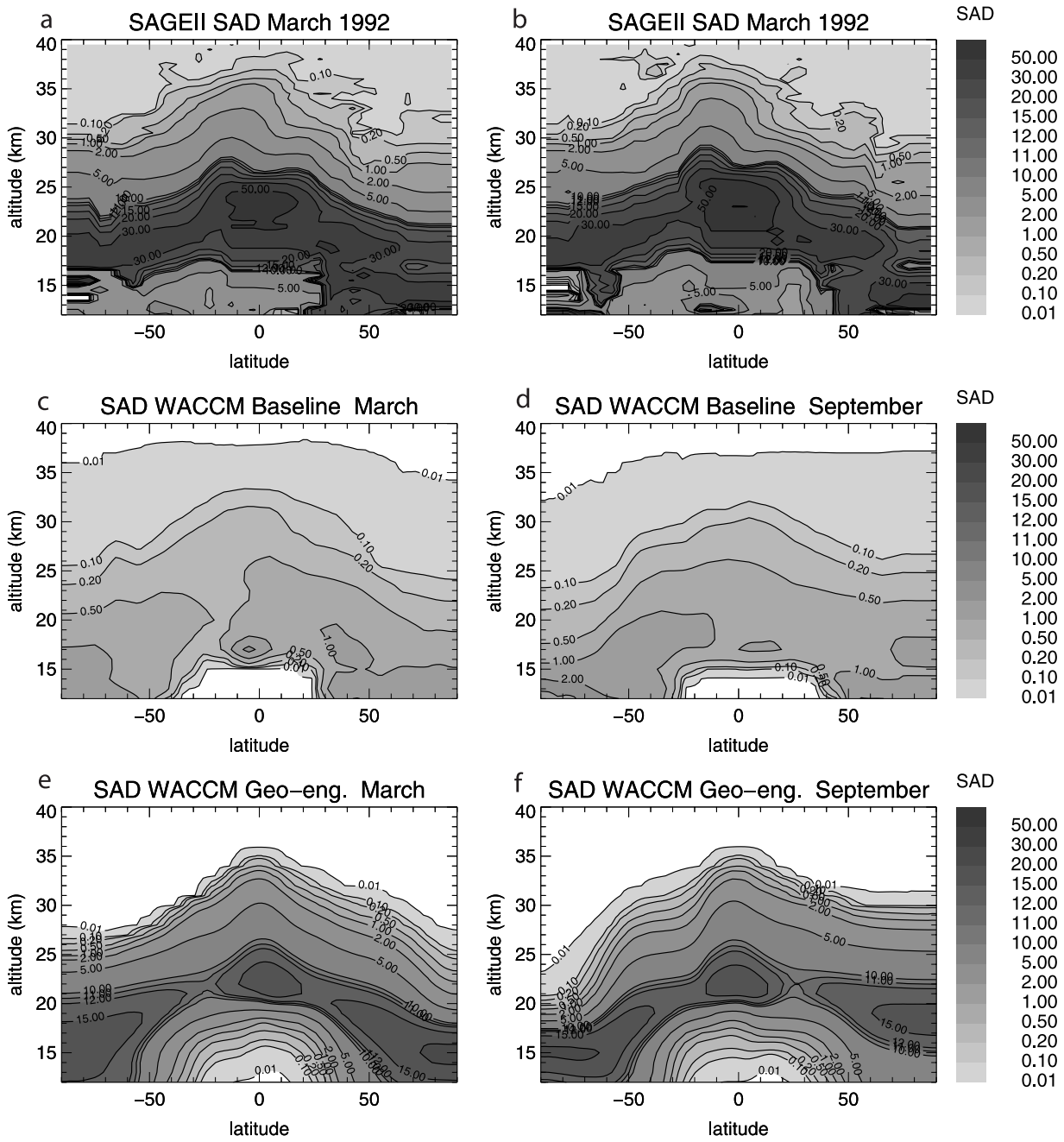

Figure 2. Surface area density from SAGE II observations for (a) March 1992 and (b) September 1992 in $\mu m^2/cm^3$ [*Thomason et al.*, 1997]. Surface area density from (c and d) WACCM3 baseline run and (e and f) WACCM3 geoengineering run for (left) March and (right) September.

aerosols, a microphysical aerosol model would need to be included into WACCM, which is beyond the scope of this paper.

[17] The monthly mean SAD in both model simulations is repeated identically for each year from 2020 onward. The purpose of this simulation is to study the impact of a fixed amount of sulfur loading for atmospheric conditions between 2020 and 2050 in the stratosphere in an effort to evaluate the consequences of geoengineering. Once the impact of sulfate aerosols on the climate including stratospheric processes is understood in more detail, further simulations can be set up, for example, a slow ramp-up of sulfate aerosols, including mitigation scenarios [*Wigley*, 2006].

[18] Figure 2 illustrates the amount of SAD for the baseline run and the geoengineering run in comparison to the SAD amount observed in the year 1992 after the eruption of Mount Pinatubo, for March and September 1992. At that time, SAD values above 50 $\mu m^2/cm^3$ in the tropics and around 20–30 $\mu m^2/cm^3$ in high latitudes between 16 and 20 km in the Southern Hemisphere (SH) and between 13 and 20 km in the Northern Hemisphere (NH) were observed. For the baseline run, SAD peaks in high latitudes below 15 km with a value of 2 $\mu m^2/cm^3$. The

geoengineering case, on the other hand, has a similar distribution as in 1992. However, maximum values are less than half compared to 1992, and reach 15 $\mu m^2/cm^3$ in the tropics at 22–25 km and in high latitudes below 20 km. In general, SAD in the geoengineering model simulation shows a distribution of larger values toward lower altitudes in polar regions in spring compared to observations during the year after the eruption of Mount Pinatubo.

3. Impact of Climate Change and Geoengineered Aerosols on Global Temperatures and Climate

[19] Temperature changes in the future atmosphere are the result of interactions between different factors. Increasing greenhouse gases directly affect atmospheric temperatures and were shown to result in an acceleration of the stratospheric circulation in WACCM, as discussed in detail by *Garcia and Randel* [2008]. Further, the decreasing halogen content in the stratosphere influences chemical processes and results in changes of trace gases such as ozone. In the case of geoengineered aerosols, additional processes affect atmospheric conditions. Strongly enhanced sulfate aerosols impact temperatures and heterogeneous processes in the lower stratosphere. In this section, we discuss the main changes of annual mean zonally averaged global and tropical temperatures in the period between 2010–2020 and 2040–2050 for both baseline and geoengineering runs (Figure 3). Differences between the geoengineering run and the baseline run in 2040–2050 are also discussed.

3.1. Global Temperature Changes

[20] For the baseline run, increasing greenhouse gases between 2010 and 2050 in the atmosphere result in a significant decrease of stratospheric temperatures with maximum decrease of 2.5 K around 40 km. A corresponding warming occurs in the troposphere with a maximum of about 1 K around 11 km in the tropics (Figure 3a). On the other hand, annually averaged temperatures in the Antarctic lower stratosphere increase significantly by up to 4 K. This is a result of increasing ozone, which follows from the decreasing halogen content in the stratosphere (see section 5). The increasing ozone absorbs radiation in the infrared and thus acts as a source of heat.

[21] For the geoengineering run, the strongly enhanced loading of volcanic-sized aerosol particles impacts directly and indirectly the dynamics and chemistry in the entire atmosphere (section 5). Volcanic-sized aerosols, as used in this simulation, absorb terrestrial longwave and solar near-infrared radiation. Besides the tropospheric cooling, aerosols cause a heating of the stratosphere, especially in the layer with enhanced aerosols (Figure 3b). Figure 3c illustrates the difference of the annual and global, zonal mean temperatures between the baseline and volcanic run in 2040–2050. The temperature signal is clearly apparent. Indeed, the constant loading of geoengineered aerosols specified here results in a cooling of the troposphere in 2040–2050 slightly below 2010–2020 conditions. On the other hand, the heating of the stratosphere, especially between about 20–30 km in middle and low latitudes, counteracts the cooling of the stratosphere due to increasing greenhouse gases (Figure 3b). In the upper stratosphere, the influence of the geoengineered aerosol layer becomes small and temperature changes between 2010–2020 and 2040–2050 are similar in both simulations.

[22] In the polar lower stratosphere, decreasing halogen concentration between 2010 and 2050 result in increasing ozone and temperatures in that region. The signal is weaker for the geoengineering run than for the baseline run owing to changing dynamics and the effect of enhanced chlorine activation on ozone (see sections 5 and 6 for more details).

3.2. Tropical Temperature Changes

[23] The temperature response of fixed geoengineered aerosols between 2020 and 2050 in comparison to the baseline model run is most pronounced and statistically significant in the tropics, on the basis of Student's *t* test. The influence of volcanic aerosols on tropical temperatures changes with altitude.

[24] For the baseline run, temperatures increase steadily in the tropical troposphere and decrease in the tropical stratosphere (Figure 4). The temperature near the Earth's surface increases by 0.2 K/decade. Around 11 km, the temperature trend reaches its maximum of 0.38 K/decade. In the stratosphere, a significant negative trend around −0.5 K/decade occurs between 20 and 30 km and an even larger trend of −0.8 K/decade is seen in the upper stratosphere (around 40 km). Temperatures at the tropopause do not change in this simulation; however, the thermal tropopause location in the tropics shifts upward by about 1 km.

[25] In contrast, the geoengineering simulation does not show a monotonic temperature evolution. With the start of geoengineering in 2020, following the abrupt change of incoming solar radiation at the Earth's surface, tropospheric temperatures decrease for 5 years until they stabilize at about −0.8 K near the surface and −2 K near 10 km compared to the baseline run. The stabilization of tropospheric temperatures after 5 years is the result of the influence of the ocean. It reflects the time scale of the response of the surface layers of the ocean to the aerosol-induced change in incoming radiation. A slow ramp-up of the amount of aerosols in the atmosphere would modify the details of the response. However, the main point is that, in a model with a coupled ocean, the response of the troposphere is not instantaneous but follows the evolution of the ocean temperature perturbation.

[26] For the next 25 years, tropospheric temperatures for the geoengineering experiment remain smaller than in the baseline run by a constant value, and follow the same trend as in the baseline run from 2025 on. In the stratosphere (around 30 km), an abrupt warming of 1.2 K occurs as a result of the enhanced SAD values in 2020. The change is almost instantaneous since the radiative budget at these altitudes is not influenced by ocean temperatures. After this initial change, the stratospheric temperatures follow a decreasing trend, since the effect of increasing greenhouse gases cool the stratosphere. In the upper stratosphere (around 40 km) geoengineered aerosols have little impact owing to their negligible abundance in this layer.

[27] In summary, the injection of a fixed amount of aerosols cools the troposphere by a certain amount, which is realized after about 5 years owing to the thermal inertia of the coupled slab ocean model. However, steadily increasing greenhouse gases in both the baseline and the geoengineered aerosol runs impact temperatures in the same way,

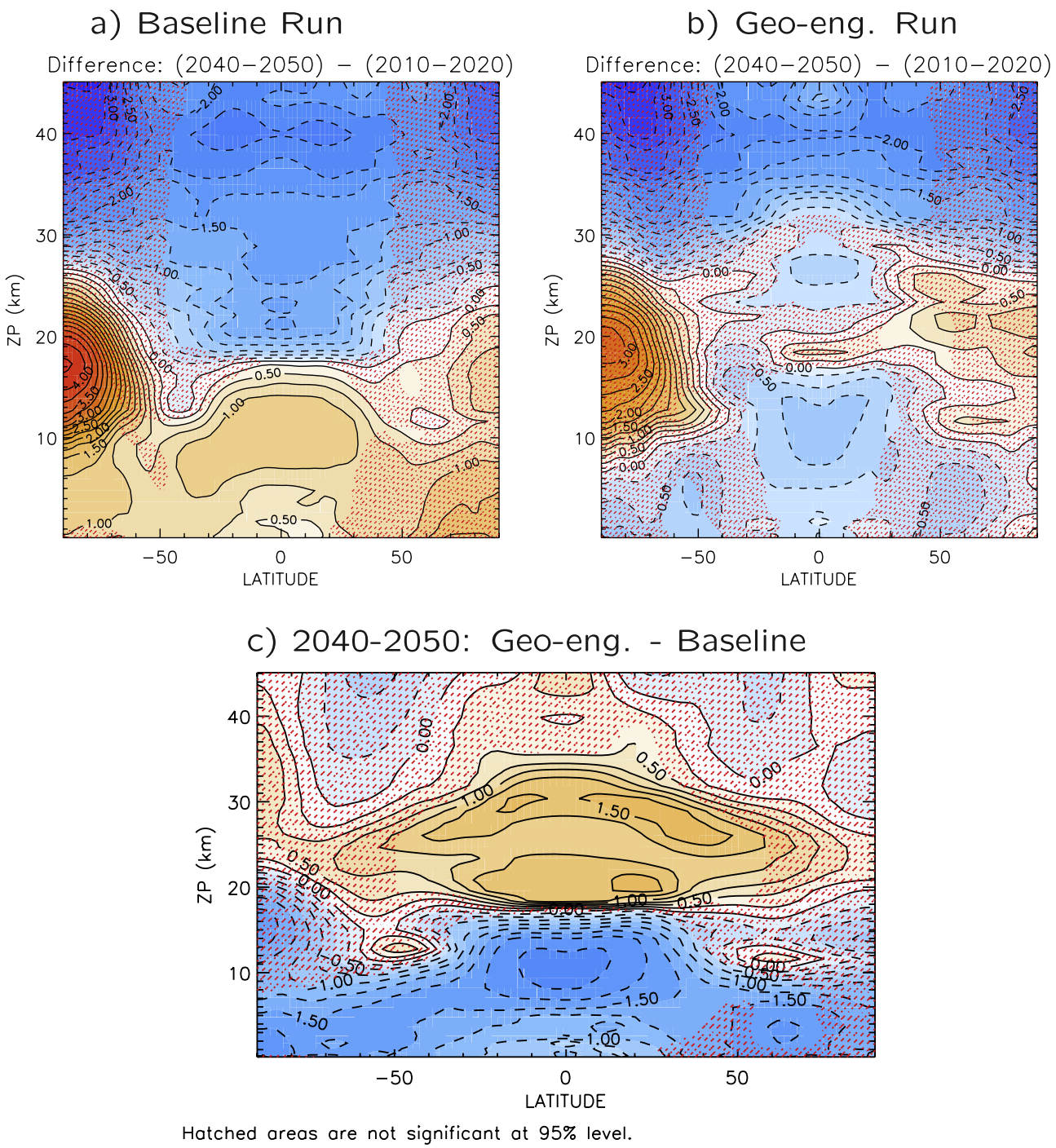

Figure 3. Annual mean, zonally averaged global temperature difference between present day (2010–2020) and future (2040–2050) for (a) the baseline run and (b) the geoengineering run. (c) Annual mean, zonally averaged global temperature difference between geoengineering and baseline runs for future (2040–2050) conditions. Hatched areas are not significant at 95% level based on Student's *t* test.

since the abundance of geoengineered aerosols is constant. The cooling achieved in the case of geoengineering would eventually be overwhelmed by increasing greenhouse gases of the IPCC A1B emission scenario, unless the content of aerosols in the stratosphere were adjusted. In our case, geoengineering delays global warming by approximately 40 years, as can be appreciated from Figure 4. Therefore, the constant injection of 2 Tg S per year of volcanic-sized aerosols is shown to counteract global warming through about 2050 with respect to the situation in 2010.

4. Impact of Geoengineered Aerosols on Surface Temperatures and Climate

[28] Increasing greenhouse gases result in increasing tropospheric and decreasing stratospheric temperatures.

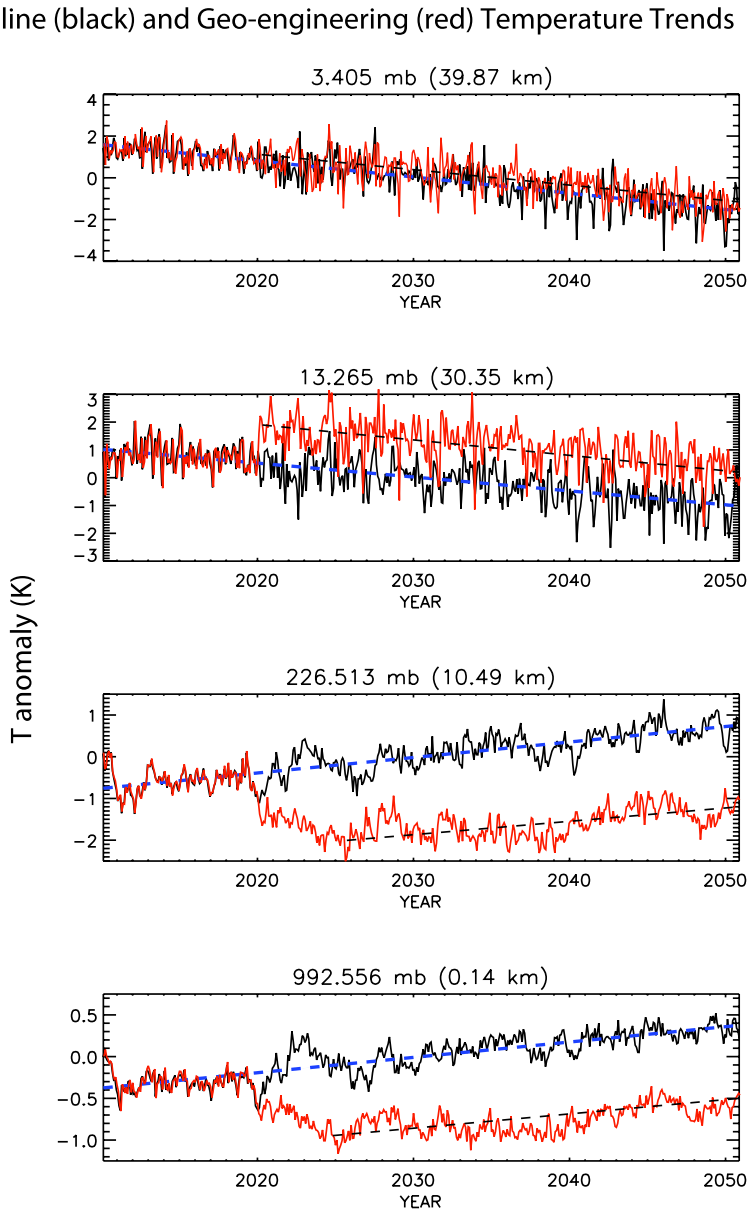

Figure 4. Temperature anomalies (between 2010 and 2050) for the geoengineering run (red) starting in 2020, and the baseline run (black) in the tropics (between 22°N and 22°S) for different altitudes. The reference state is the mean temperature of the baseline model simulation between 2010 and 2050.

The additional impact of the scattering of short-wave radiation due to enhanced volcanic-sized geoengineered aerosols in the stratosphere results in a cooling of the troposphere and the surface. In this section, differences between the baseline and the volcanic aerosol run in surface temperatures, precipitation and sea ice are described. Temperature changes are also compared to results using the Community Atmosphere Model (CAM).

4.1. Surface Temperature Changes Between 2010–2020 and 2040–2050

[29] Climate models predict surface temperatures to increase from present day conditions by about 1–3 K by 2050 as a result of increasing greenhouse gases, with considerably larger warming in the polar regions [*IPCC*, 2007]. For the WACCM3 baseline model simulation (Figure 5, top), temperatures increase globally by about 1 K between 2010–2020 and 2040–2050 and, consistent with IPCC results, the largest warming of the surface occurs in high latitudes, especially in winter for each hemisphere. The ice-albedo feedback is regarded as important in accelerating the warming in the Arctic. In addition, a recent study by *Cai* [2005] used a four-box set of radiative-convective models coupled by parameterized transport across the boxes to show that heat transport by the atmospheric circulation also plays a significant role in the enhancing polar warming.

[30] The geoengineered aerosol implemented in the model run cools the surface by about 0.5 K between 2010–2020 and 2040–2050 (Figure 5, bottom). Changes in higher

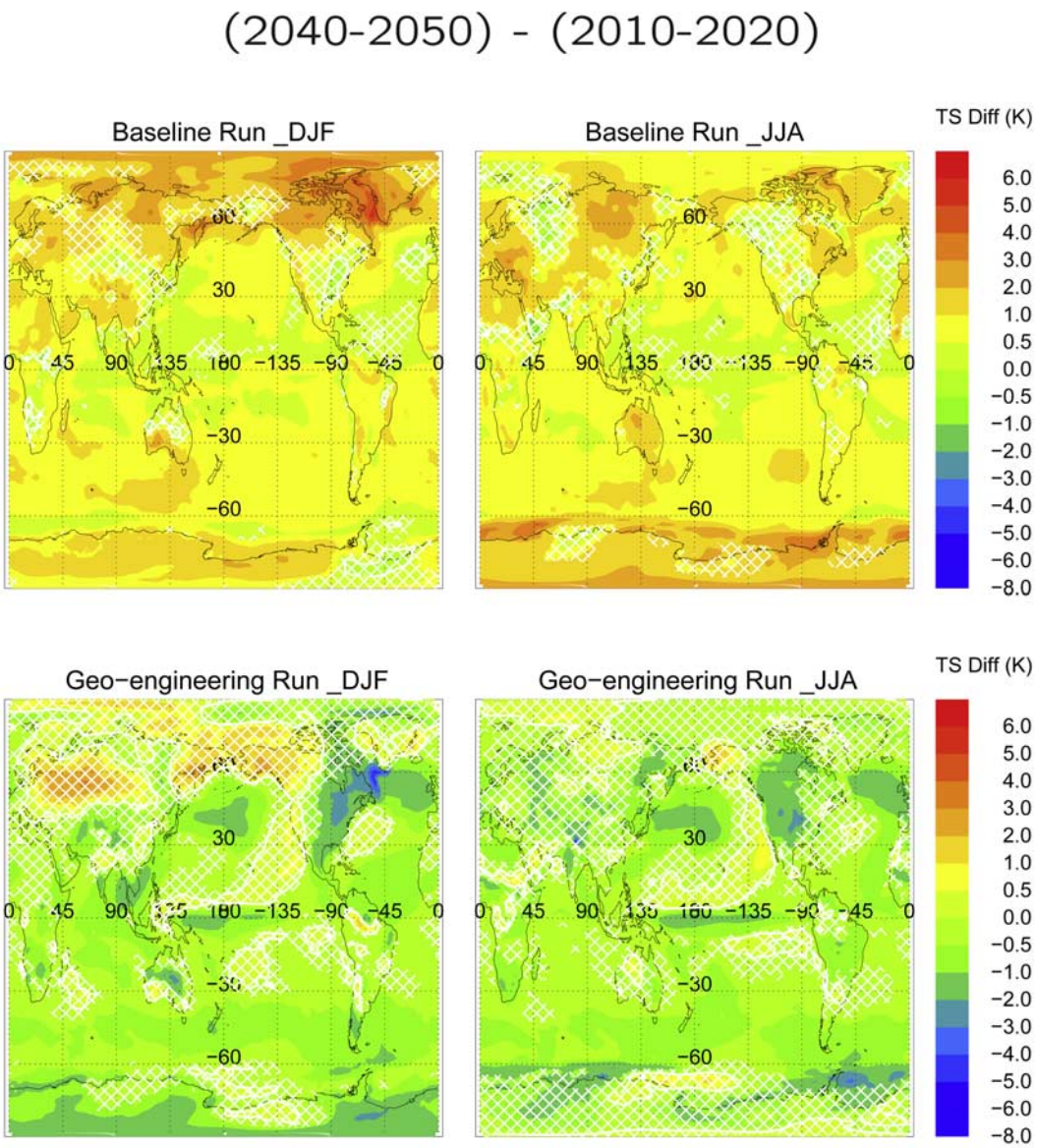

Figure 5. Difference of surface temperatures between future (2040–2050) and present-day (2010–2020) conditions for (top) the baseline run and (bottom) the geoengineering run. (left) Winter results (December, February, and March averages) and (right) summer results (June, July, and August averages). Zero line is indicated in white. Hatched areas are not significant at 95% level based on Student's *t* test.

latitudes, especially in the Northern Hemisphere, are not statistically significant. In general, the climate in 2040–2050 including geoengineering is much more similar to 2010–2020 than the climate without geoengineering according to Student's *t* test. However, temperatures do not change uniformly between present and future in the case of geoengineering but local changes up to 3 K occur, as also simulated by *Robock et al.* [2008].

4.2. Comparison Between WACCM and CAM

[31] In Figure 6 (top), surface temperature differences between geoengineering and the baseline runs in WACCM3 for the period 2040–2050 are shown for the NH winter season (Figure 6, top left) and for the NH summer season (Figure 6, top right). Geoengineered aerosols result in a cooling of the Earth's surface of 1.2 K globally on an annual average, with around 1 K cooling in the tropics (see Figure 4), and increasing cooling toward higher latitudes in WACCM3.

[32] A similar cooling was found in a geoengineering model study by *Robock et al.* [2008], who used a comprehensive atmosphere-ocean general circulation model to consider the impact of the injection of 5 Tg S/a on Earth's surface temperatures. This aerosol size distribution was similar to that used here; however, only limited stratospheric chemistry was included in that model simulation. Even though the amount of aerosol injected was much larger in the work by *Robock et al.* [2008] than in our simulation, a similar cooling at the Earth's surface was found. Since *Robock et al.* [2008] assumed an A1B future scenario, changes in stratospheric circulation and the resulting faster removal of stratospheric aerosols might require a larger

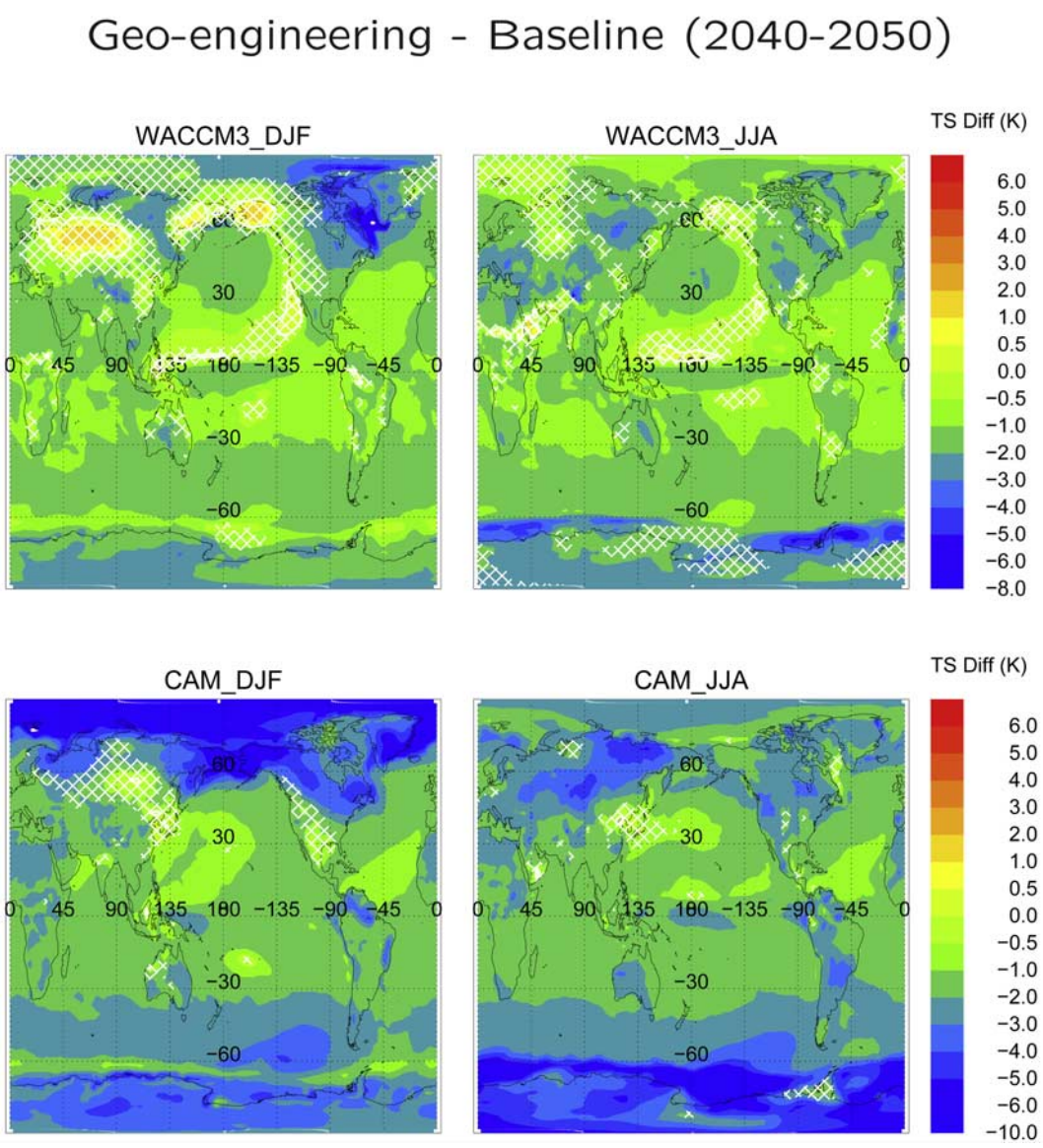

Figure 6. Difference of surface temperatures between geoengineering and baseline runs. (top) WACCM3 results for the period 2040–2050 are shown. (bottom) CAM model result for the same aerosol distribution and for present-day CO_2 conditions are shown. (left) Winter results (December, February, and March averages) and (right) summer results (June, July, and August averages). Zero values are indicated in white. Hatched areas are not significant at 95% level based on Student's *t* test.

annual injection amount to maintain the same aerosol layer in the stratosphere. Here, we use a fixed SAD distribution that is based on the present-day stratospheric circulation.

[33] Further, *Robock et al.* [2008] simulated a weaker cooling in the winter polar regions, especially in the SH. Enhanced heterogeneous chemistry in our simulation and therefore a deeper ozone hole in case of geoengineering (as shown below), might be responsible for the stronger cooling in high polar latitudes found here.

[34] We also compare our results with the results of a CAM model simulation performed earlier [*Rasch et al.*, 2008b]. In Figure 6 (bottom), the surface temperature changes are shown for a CAM simulation that used the same geoengineered aerosol distribution, called "volc2" by *Rasch et al.* [2008b]. CAM is a climate model related to WACCM but there are several important differences. Unlike WACCM3, CAM does not simulate changes in stratospheric chemistry and, therefore, it does not simulate changes in the ozone distribution that affect the heating rates in the atmosphere. The ozone distributions are prescribed and invariant to the changing climate. This may have a significant impact on the tropospheric dynamical response [e.g., *Kiehl et al.*, 1988; *Thompson and Solomon*, 2002; *Perlwitz et al.*, 2008; *Son et al.*, 2008]. The CAM model also uses a different approach to calculate the slab ocean meridional and deep ocean heat transport (the "Q fluxes") than WACCM, which may explain some of the differences highlighted below.

[35] Different than here, the differences between the geoengineering and baseline model runs in CAM are calculated for present-day CO_2 conditions. We have shown earlier (Figure 4) that the temperature offset between the

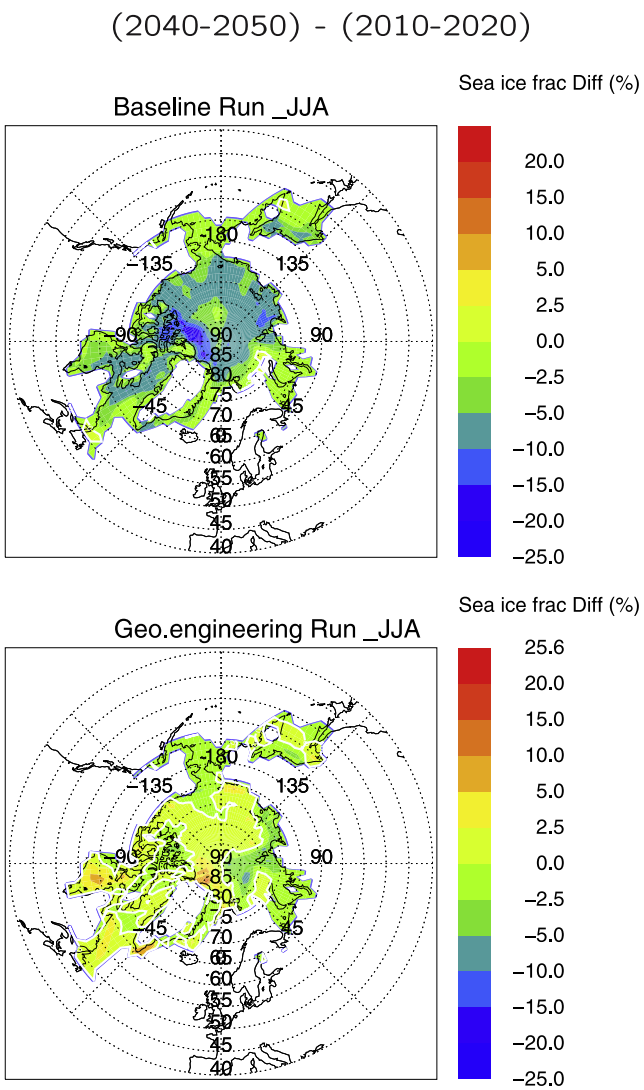

Figure 7. Difference of NH summer (June, July, and August averages) sea ice concentration between future (2040–2050) and present-day (2010–2020) conditions for (top) the baseline run and (bottom) the geoengineering run.

geoengineering and baseline model runs is independent of the period considered for a constant amount of SAD in the stratosphere. Therefore, a comparison of temperature anomalies (geoengineering run minus baseline run) between WACCM3 for 2040–2050 and CAM for present-day conditions is reasonable.

[36] In CAM, a SAD distribution identical to the one used in the WACCM3 simulation results in an annual mean global cooling of 2.0 K averaged over the Earth's surface, compared to baseline conditions. As in WACCM3, the cooling is smallest at lower latitudes and increases toward high latitudes. However, the cooling in CAM as a result of enhanced geoengineered aerosols is much stronger and more broadly statistically significant at high latitudes in winter than in WACCM3. This highlights the different behavior of the stratosphere in polar regions in high-top versus conventional models. A detailed investigation about the different temperature response in the two models will be the subject of future studies.

4.3. Sea Ice and Precipitation Changes Between 2010–2020 and 2040–2050

[37] In WACCM3, increasing temperatures in the baseline run result in a 15% decrease of the sea ice fraction between 2010–2020 and 2040–2050, especially in the summer NH (Figure 7). In contrast, the impact of geoengineered aerosols produces a cooling of the surface between 2010–2020 and 2040–2050, so that the change in sea ice fraction between 2010 and 2050 is much smaller and of variable sign (±5%). On average, the cooling of the troposphere due to the specified geoengineered aerosol loading would result in a slightly greater sea ice fraction in both hemispheres in 2040–2050 compared to 2010–2020.

[38] Another important climate variable is precipitation. The precipitation rate is strongly influenced by the incoming radiation and the water vapor content of the troposphere. Increasing surface temperatures as a result of changing greenhouse gases in the atmosphere result in a larger water vapor content in the troposphere [*IPCC*, 2007]. The resulting stronger Hadley circulation and the changing hydrological cycle tend to increase the annual precipitation at the equator and decrease it in the subtropics. For the baseline run, a very minor increase of global precipitation occurs between 2010–2020 and 2040–2050 with less than 0.1 mm/d increase over land and ocean (see Figure 8, top).

[39] For the geoengineering model run decreasing tropospheric temperatures and, therefore, a weaker radiative forcing compared to the baseline run results in a weaker Hadley cell and a reduction of precipitation near the equator (Figure 8, bottom). Compared to 2010–2020, the global averaged precipitation is reduced by less than 0.1 mm per day. However, precipitation decreases in the tropics by 0.5–0.8 mm per day over land and ocean, and increases in the subtropics. Therefore, geoengineering in this simulation does not result in a precipitation pattern similar to present-day conditions, but instead leads to a slightly dryer climate, especially around the equator. We note, that as for the baseline run, small changes are not significant in the period considered owing to the large interannual variability. In the geoengineering run, the statistically significant precipitation decreases in the tropics come mainly from the NH winter season (DJF), and are dominated by changes in the Pacific and Indian oceans, and over the maritime continent (not shown).

5. Stratospheric Dynamics and Chemistry

[40] Increasing tropospheric temperatures and decreasing stratospheric temperatures between 2010 and 2050, which are a result of increasing greenhouse gases, produce chemical and dynamical changes in the stratosphere that are strongly coupled. The addition of geoengineered aerosols to the climate system has an additional impact on temperatures, chemistry and the wind field, and therefore on the global ozone column. In this section, we discuss in detail the contribution of chemical and dynamical changes on ozone as a result of increasing greenhouse gases and additional geoengineered aerosols in the stratosphere. At the end of the section, we discuss changes in the depth of the ozone column, important for the amount of UV radiation reaching the Earth's surface.

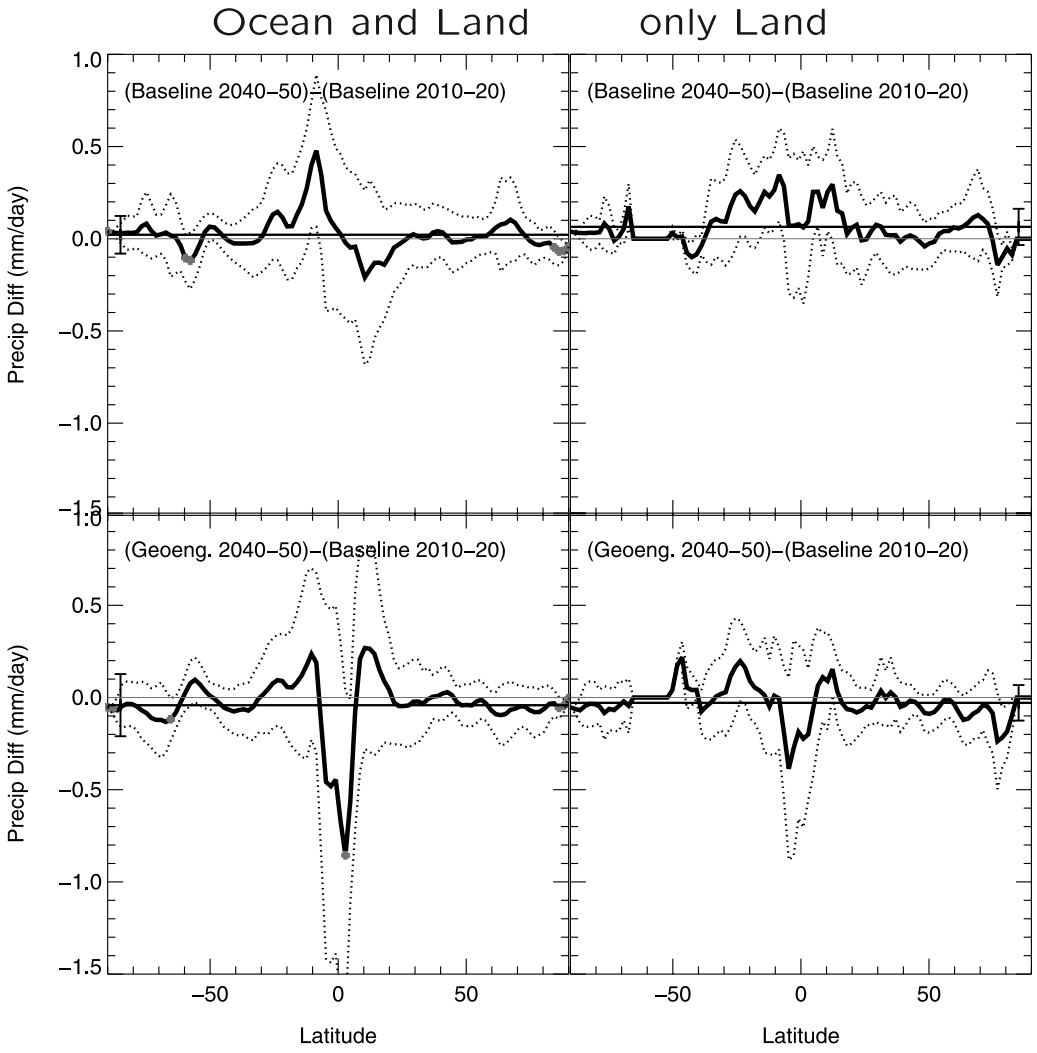

Figure 8. Difference of annual cumulative precipitation in mm/d between future (2040–2050) and present-day (2010–2020) conditions for (top) the baseline run and (bottom) the geoengineering run. Annual mean zonal averages (thick black curves) are shown (left) over ocean and land and (right) over the land only. Significant changes between future and present-day fields are denoted by grey dots superimposed on the precipitation difference curves. The standard deviation as a result of the annual variability at each latitude is shown as dotted lines. Global mean changes are shown as grey lines with their standard deviation indicted by the error bar.

5.1. Global Annual Mean Changes of Stratospheric Ozone

[41] The global changes of zonally averaged ozone mixing ratios between 2010–2020 and 2040–2050 for both the baseline and the geoengineering model runs are shown in Figures 9a and 9b. Further, differences between the geoengineering and the baseline runs in 2040–2050 are shown in Figure 9c.

[42] Decreasing temperatures in the stratosphere as a result of increasing greenhouse gases slow down ozone destroying cycles and therefore result in increasing ozone mixing ratios in the upper stratosphere (35–45 km) and larger ozone values in 2040–2050 compared to 2010–2020 (see Figure 9, top). At high latitudes, decreasing abundances of halogen compounds result in reduced chemical ozone depletion by 2040–2050, especially in high polar latitudes of the SH. In the tropical lower stratosphere below about 28 km, ozone production rates decrease owing to increases in ozone at higher altitudes, which reduce UV radiation reaching the lower stratosphere. In addition, there are changes in tropical upwelling which lead to an increase in the vertical advection of ozone-poor air.

[43] Strongly enhanced aerosols in the geoengineering run result in a significant increase of ozone mixing ratios in the upper part of the aerosol layer at all latitudes compared to the baseline simulation (Figure 9, bottom). On the other hand, in the geoengineering run ozone mixing ratios are significantly smaller around 25 km in the tropics and below 20 km in high southern latitudes compared to the baseline run. A detailed discussion of these differences is given in section 5.2.

5.2. Impact of Geoengineered Aerosols on Chemistry and Dynamics

[44] The reduction of tropospheric warming in the geoengineering run is expected to lead to a weaker Brewer-

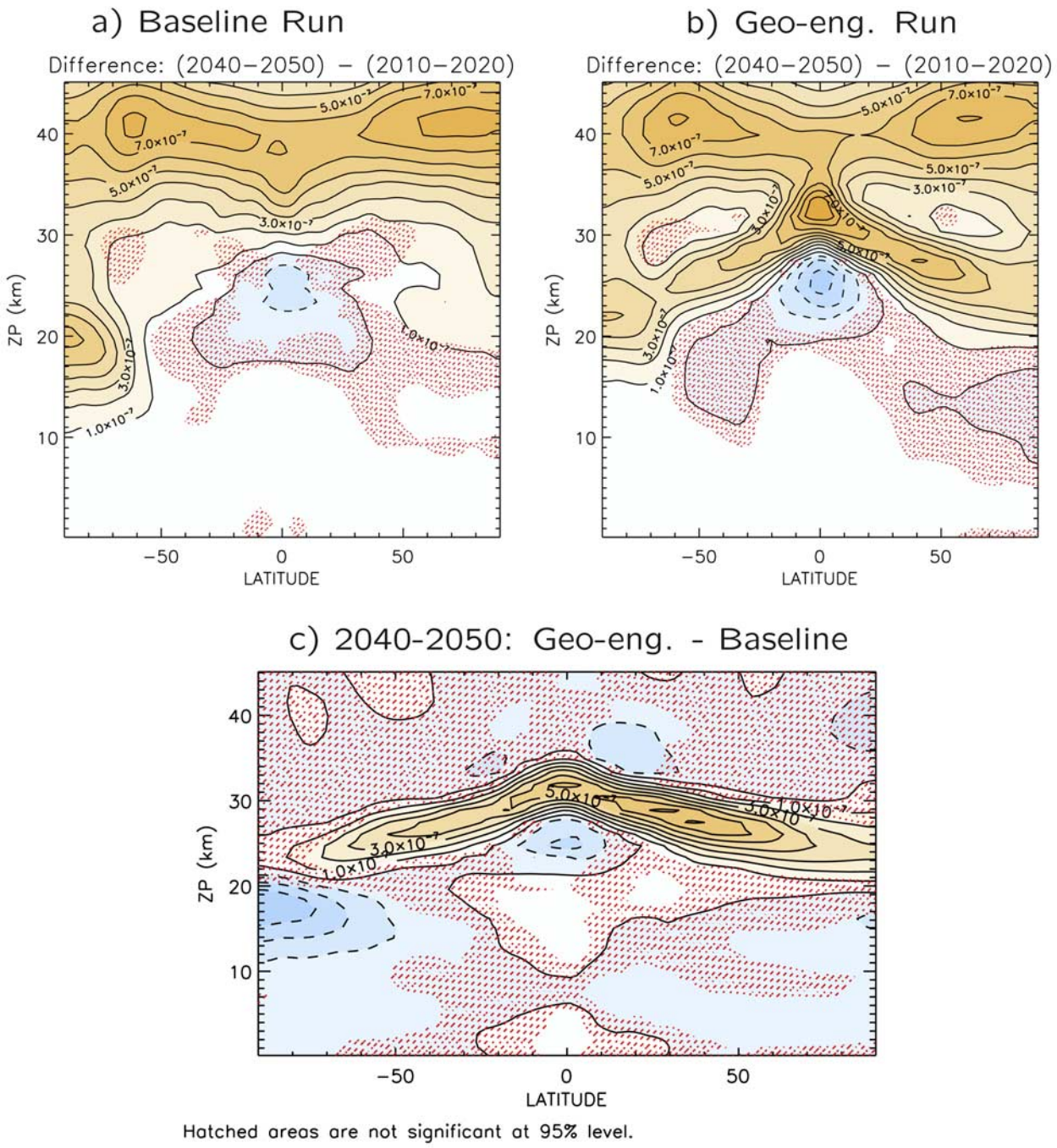

Figure 9. Difference of annual mean zonally averaged global ozone values between present day (2010–2020) and future (2040–2050) for (a) the baseline run and (b) the geoengineering run. (c) Difference of annual mean zonally averaged global ozone values between geoengineering and baseline runs for future (2040–2050) conditions. Hatched areas are not significant at 95% level based on Student's *t* test.

Dobson circulation in the lower stratosphere compared to the baseline run [*Garcia and Randel*, 2008]. Further, the strongly enhanced SAD in the stratosphere results in a significant increase in heterogeneous processing globally [*Tabazadeh et al.*, 2002] and in enhanced chlorine activation in the winter polar vortices [e.g., *Drdla*, 2005; *Tilmes et al.*, 2008]. The impact of geoengineered aerosols on ozone production, different ozone destroying cycles, and advection is discussed below for the tropics, midlatitudes and polar regions.

5.2.1. Tropics and Midlatitudes

[45] The importance of chemical production, advection and chemical loss cycles on ozone depends on altitude and latitude. The main chemical production mechanism for ozone, the photolysis of molecular oxygen, occurs in tropical latitudes with a maximum around 40 km [e.g., *Brasseur and Solomon*, 2005]. Ozone loss takes place

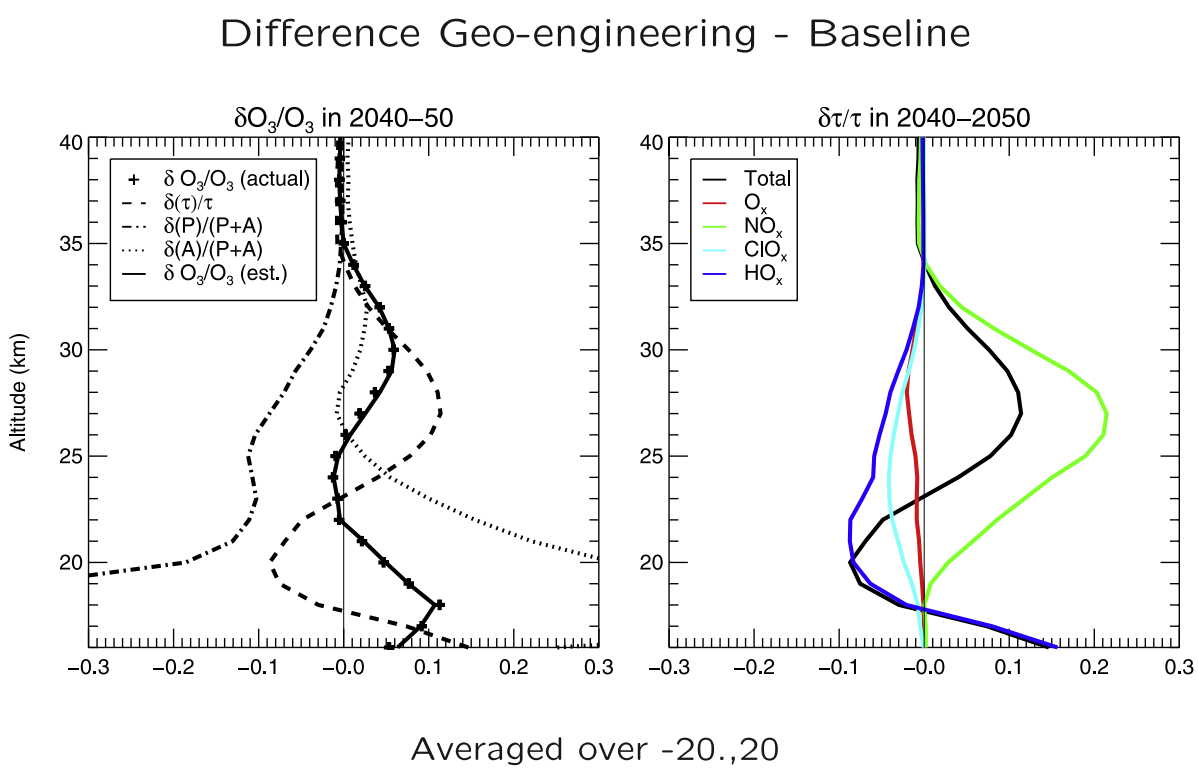

Figure 10. (left) Fractional difference $\delta O_3/O_3$, between the geoengineering run and the baseline run calculated directly from model output (plus signs) and estimated using equation (5) (solid lines). The contributions to $\delta O_3/O_3$ from fractional changes in photochemical lifetime (long-dashed line), production rate (dash-dotted line), and advection A (short-dashed line) are shown. Values are averaged between 20°S and 20°N and for the years 2040–2050, except for the production rate, which was available for 2049 only. (right) Fractional change of the O_3 chemical lifetime due to the combined effect of all the ozone catalytic cycles (black), as well as the weighted fractional changes, equation (8), due to individual cycles (different colors). See text for details.

through several catalytic cycles involving the O_x, NO_x, ClO_x, BrO_x and HO_x chemical families [*Grooß et al.*, 1999; *Metz et al.*, 2005]. The O_x cycle is important in the middle and upper stratosphere, while the HO_x cycle is most effective in the lower and upper stratosphere. The NO_x cycle dominates ozone loss in the middle stratosphere and is controlled by the NO_x/NO_y ratio [e.g., *Brasseur and Solomon*, 2005]. The NO_x cycle also interacts with the ClO_x, BrO_x and HO_x cycles and therefore depends on the amount of halogens in the stratosphere [*Fahey et al.*, 1993; *Solomon et al.*, 1996; *Tabazadeh et al.*, 2002]. Advection becomes important below about 30 km.

[46] Geoengineered aerosols impact ozone owing to changes in ozone destruction cycles, ozone production, and advection. Under certain circumstances, it is possible to estimate quantitatively the difference in annual average ozone between the geoengineering and baseline runs. Consider the continuity equation for O_x,

$$\frac{\partial O_x}{\partial t} = P + L + A, \tag{1}$$

where P, L, and A denote the production, loss, and advection rates. Over the annual cycle the time rate of change of O_x on the left-hand side of (1) is negligible compared to the terms on the right hand side of the equation. Furthermore, in the range of altitude considered here, the odd oxygen family ($O_x = O_3 + O$) is dominated by O_3, so we can rewrite (1) as

$$P + A - \frac{O_3}{\tau} \approx 0, \tag{2}$$

where we have expressed the loss term as

$$L = -\frac{O_3}{\tau}, \tag{3}$$

with τ being the photochemical lifetime of O_3. From equation (2), the annual mean equilibrium value of ozone is then

$$O_3 = (P + A) \cdot \tau, \tag{4}$$

and fractional differences in ozone, $\delta O_3/O_3$, between the geoengineering run and the baseline model run may be estimated as

$$\frac{\delta O_3}{O_3} = \frac{\delta(P + A)}{(P + A)} + \frac{\delta\tau}{\tau}, \tag{5}$$

where we have retained only terms linear in δO_3, δP, and $\delta\tau$.

[47] In Figure 10 (left) we evaluate (5) in the tropics, between ±20°. Above 28–30 km the behavior of δ O_3/O_3 is dominated by changes in the chemical lifetime of O_3. We note, in particular, that the increase in δ O_3/O_3 centered at ~30 km is attributable mainly to smaller ozone loss rates at these altitudes in the geoengineering simulation (dashed line). We show later that the reduction in ozone loss rates is dominated by a much reduced rate of NO_x catalysis.

[48] At lower altitudes, advection cannot be neglected. We are unable to compute the advection term directly from existing model output because three-dimensional fields for ozone and the horizontal and vertical velocity were not available on a daily basis, a requirement for the accurate calculation of the eddy flux terms $v'O_3'$, $w'O_3'$. Instead, we assume that A is approximately equal to the difference between production and loss, i.e., $A \approx O_3\tau^{-1} - P$. The contribution of advection becomes increasingly important below 28 km, and dominates the behavior of $\delta O_3/O_3$ below 20–22 km. At these altitudes, reduced vertical advection of ozone-poor air from the lowermost stratosphere in the geoengineering case leads to higher ozone abundances than in the baseline case. Weaker tropical upwelling is expected under geoengineering because the troposphere becomes much cooler and the mechanism for the acceleration of the Brewer-Dobson circulation, namely an enhanced planetary wave activity, proposed by *Garcia and Randel* [2008] is therefore less effective. Note finally that, in the range of altitude 22–26 km, $\delta O_3/O_3$ is negative as a result of a reduced rate of O_x production from oxygen photolysis, which in turn is due to enhanced absorption of UV radiation in the region of positive $\delta O_3/O_3$ centered at 30 km.

[49] The effect of geoengineering on the loss rates due to different catalytic cycles may be calculated by rewriting the ozone loss term, $O_3\,\tau^{-1}$, as a sum of contributions from the various cycles,

$$\frac{O_3}{\tau} = O_3 \sum_i \frac{1}{\tau_i}, \tag{6}$$

where the τ_i denote the lifetimes of O_3 with respect to the catalytic cycles for O_x, NO_x, etc. It follows that

$$\delta\tau = \delta\left(\sum_i \frac{1}{\tau_i}\right)^{-1} = \sum_i \left(\frac{\tau}{\tau_i}\right)^2 \cdot \delta\tau_i, \tag{7}$$

so that the term $\delta\tau/\tau$ in (5) may be written as

$$\frac{\delta\tau}{\tau} = \sum_i \frac{\tau}{\tau_i} \cdot \frac{\delta\tau_i}{\tau_i}. \tag{8}$$

Figure 10 (right) shows the results for the tropics (±20)°. Maximum differences in $\delta\tau/\tau$ (black curve, which is identical to the dashed curve on Figure 10 (left)) between the geoengineering and baseline runs occur within the layer of enhanced aerosol SAD, centered near 27–28 km. These differences are dominated by the NO_x cycle (which is most important in the middle stratosphere). The NO_x cycle becomes less effective in the geoengineering run because enhanced heterogeneous reactions shift the ratio NO_x/NO_y toward NO_y [e.g., *Fahey et al.*, 1993] (in particular $N_2O_5 + H_2O \rightarrow 2\ HNO_3$), with an increasing effect toward the upper region of the enhanced aerosol layer. This shift increases the photochemical lifetime of ozone with respect to NO_x, as indicated by the green curve in Figure 10 (right). The lifetimes of O_3 with respect to all the other loss cycles are somewhat shorter in the geoengineering run, and therefore tend to reduce the total photochemical lifetime rate [*Solomon*, 1999], but the increase in the lifetime with respect to NO_x is dominant for 2040–2050 halogen conditions.

[50] In midlatitudes, production and loss cycles are similarly influenced as in the tropics. As for the tropics, the increase in the photochemical lifetime of O_3 with respect to NO_x in the geoengineering case dominates changes in the total O_3 lifetime at these latitudes (not shown).

5.2.2. High Latitudes

[51] At higher latitudes (poleward of ~70°), O_3 loss varies strongly with season, being largest during local late winter and spring, when cold temperatures activate chlorine and greatly increase the loss rate due to halogens. Therefore, as opposed to the tropics and midlatitudes, we consider two seasons: January, February and March (JFM), a time when the impact of polar ozone depletion is expected to be strongest in the NH, and September, October and November (SON), when the largest impact of polar ozone depletion in the SH can be expected. It should be noted that, considering the regions north and south of 70°, we do not quantify changes in the polar vortex alone, but we average over an area inside and outside the vortex edge. Dynamical changes of the polar vortex and ozone depletion in the polar vortex are discussed in section 5.3.

[52] Over the seasonal time scales considered here (JFM and SON), ozone in the lower polar stratosphere is not in quasi steady state and the time derivative of O_x ($\approx O_3$) cannot be neglected in equation (1). Therefore, we cannot quantify the impact of chemical loss, production and advection on the changes in ozone as a result of geoengineering in the same way as done for the tropics via equation (5). Instead, we discuss here the changes of the different rates that impact seasonal changes of ozone and therefore contribute to changes in ozone values as a result of geoengineering.

[53] Changes of the total loss rates between geoengineering and baseline runs are shown in Figure 11 (left). As for the tropics and midlatitudes, differences in the ozone loss rates between the geoengineering and baseline runs are mainly the result of enhanced heterogeneous reactions in the region of enhanced SAD in the geoengineering run. Thus, NO_x catalysis becomes less effective at high latitudes in the range of altitude 20–25 km. This is reflected in Figure 11 by a positive anomaly in the geoengineering minus baseline loss rate centered around 22–24 km (green curves). Above 25 km in the SH, there are also large changes in the NO_x cycle, which are not statistically significant and result from large natural variability due to downward transport of NO_x likely produced by energetic particle precipitation in the mesosphere [*Marsh et al.*, 2007]. In addition, enhanced aerosols accelerate ozone loss due to halogen (ClO_x and BrO_x) catalysis in the range of altitude 12–22 km, seen as a negative difference in the halogen loss rates (cyan curves), between the geoengineering and baseline cases.

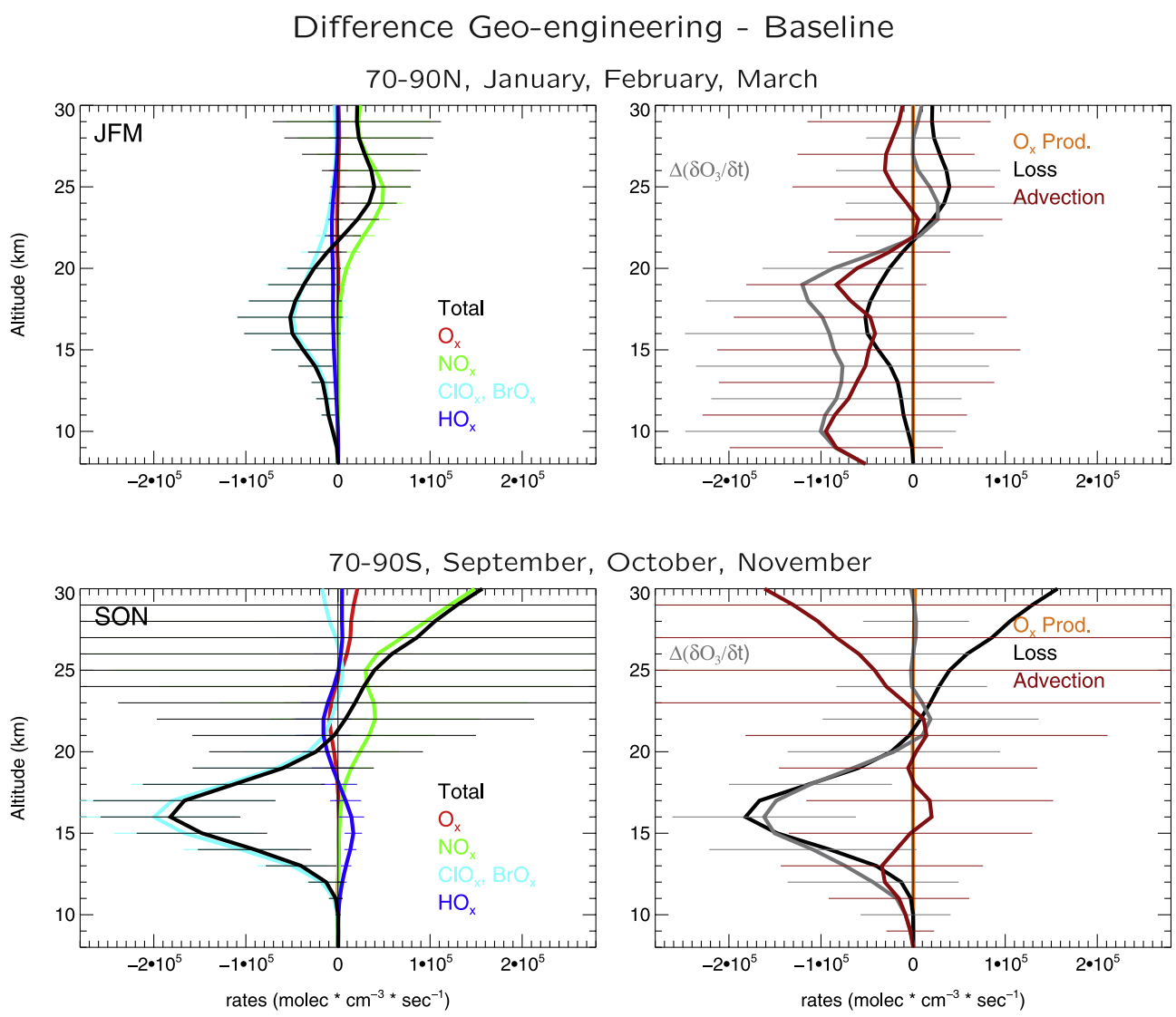

Figure 11. (left) Difference between geoengineering and baseline in the ozone destruction rate due to individual catalytic cycles (colors) and in the total destruction rate (black line). (right) Difference between geoengineering and baseline in ozone loss rate, production rate, advection rate, and time rate of change, $\partial O_3/\partial t$. The results show 2040–2050 averages for high latitudes poleward of 70°, for different seasons. The standard deviation of the 10-year average is indicated by the error bars. Ozone production rates were available for 2049 only, so error bars are not shown.

[54] In Figure 11 (right), we compare differences in ozone production and loss rates, advection, and time rate of change, $\partial O_3/\partial t$, between the geoengineering and baseline runs for the same seasons as in Figure 11 (left) (JFM in the NH and SON in the SH). The loss rates shown are the total of all the catalytic cycles and thus correspond to the black lines in the left hand panels. For the SH in SON, the difference between geoengineering and baseline in $\partial O_3/\partial t$ (gray lines) is dominated by the effect of enhanced ozone destruction in the geoengineering case (which itself is due mainly to faster halogen catalysis, as discussed above). In the NH during JFM, on the other hand, the difference between geoengineering and baseline in $\partial O_3/\partial t$ has important contributions from both differences in ozone loss rates and differences in advection. However, differences in advection are for the most part not statistically significant (large red error bars, Figure 11, right).

[55] In summary, in the period considered (2040–2050), significant changes in the rate of ozone loss occur as a result of geoengineering in the polar regions of the SH, centered around 16–17 km, owing to faster halogen catalysis. Changes in advection are negligible in the SH in SON; they are larger but not statistically significant in the NH during JFM. The differences in ozone loss rates between the geoengineering and baseline cases impact the behavior of column ozone, as shown next.

5.3. Changes in Column Ozone

[56] The depth of the ozone column in the atmosphere is controlled by chemistry and transport. The stratospheric mean meridional circulation transports ozone from the

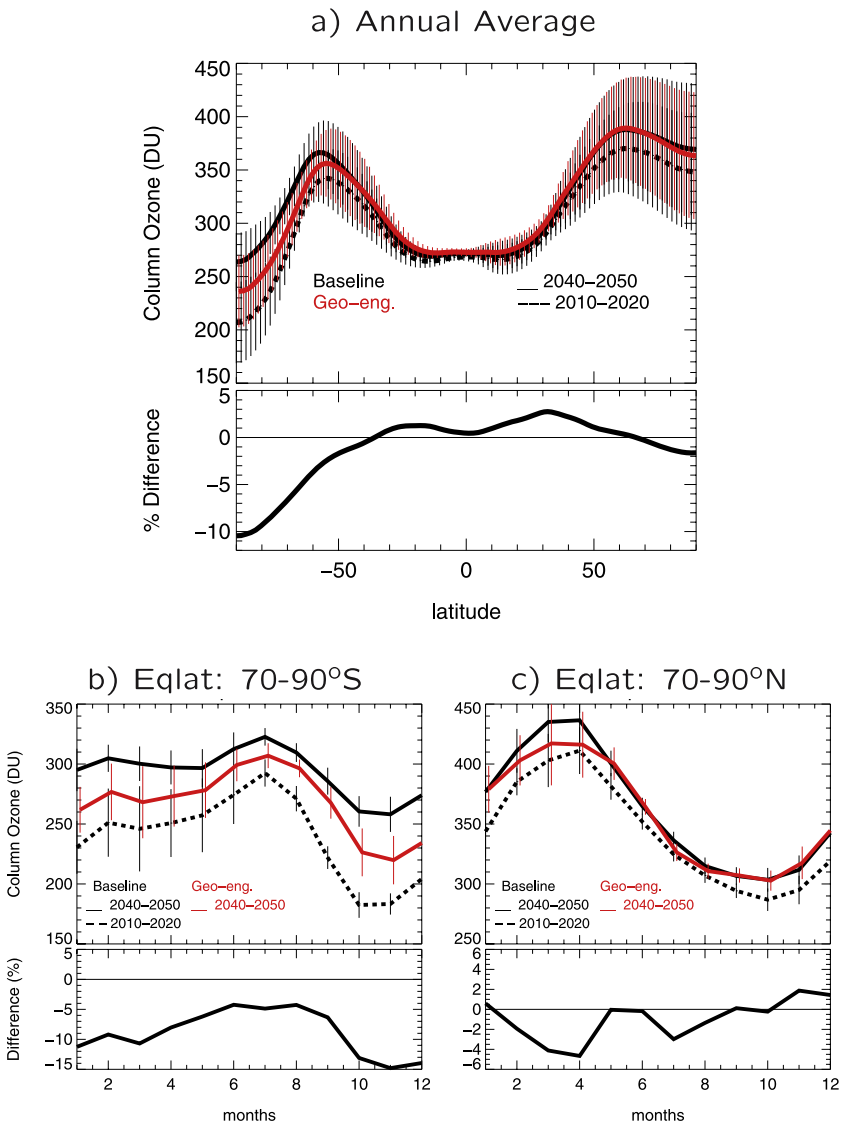

Figure 12. (a) (top) Decadal averages (dashed line, 2010–2020; solid line, 2040–2050) of column ozone (DU) as functions of latitude for the baseline (black line) and geoengineering (solid red line, 2040–2050) runs, including the standard deviation (error bars), as well as (bottom) the difference for 2040–2050. (b) (top) Decadal averages (dashed line, 2010–2020; solid line, 2040–2050) of column ozone (DU) averaged between 70°S and 90°S equivalent latitudes for baseline (black line) and geoengineering (solid red line, 2040–2050) runs, including the standard deviation (error bars), as well as (bottom) the differences for 2040–2050. (c) (top) Decadal averages (dashed line, 2010–2020; solid line, 2040–2050) of column ozone (DU) averaged between 70°N and 90°N equivalent latitudes for baseline (black line) and geoengineering (solid red line, 2040–2050) runs, including the standard deviation (error bars), as well as (bottom) the differences for 2040–2050.

tropics to middle and high latitudes. On a global annual average, the ozone column (Figure 12a, top plot) shows maximum values in middle and high latitudes of the NH. Significantly smaller column ozone values occur in high latitudes of the SH in winter and spring, where ozone depletion is most important owing to halogen activation in winter and spring (as discussed above). For high northern latitudes, WACCM3 underestimates polar ozone depletion compared to observations in the 1990s [*Tilmes et al.*, 2007] and results have to be considered with caution.

[57] In Figure 12a, annual mean zonally averaged column ozone for the periods 2010–2020 and 2040–2050 is compared. Further, ozone column values from the geoengineering model run are compared to values derived from the baseline run for 2040–2050. The difference between the geoengineering run and the baseline run is shown in Figure 12a (bottom).

[58] Between 2010–2020 and 2040–2050, column ozone in middle and high latitudes increases up to 10% in the geoengineering case and up to 25% in the baseline simulation. With increasing greenhouse gases, colder temperatures result in a slowdown of the ozone destroying cycles in the upper stratosphere, and therefore a higher equilibrium mixing ratio in the ozone source region and a concomitant

increase in ozone transport to middle and high latitudes, as discussed above. Furthermore, the decreasing halogen content in 2040–2050 compared to 2010–2020 in the stratosphere contributes to increasing ozone values in the upper stratosphere and results in significantly less ozone depletion in 2040–2050 compared to earlier periods in high latitudes in the SH. In high latitudes in the NH, changes between 2010–2020 and 2040–2050 are small compared to the interannual variability during the 10 years considered.

[59] In the geoengineering case, the combination of increasing heterogeneous reaction rates and changes in dynamics influence the ozone mixing ratios compared to the baseline run (as discussed in section 5.2). On average near the equator (between 10°N and 10°S), the depth of the ozone column shows little change. In the region between about 10°–30° north and south, the impact of different processes on ozone at different altitudes results on average in slightly (up to 2%) larger column ozone values in the geoengineering case compared to the baseline run. In high southern latitudes, the annually averaged column ozone for the geoengineering run is up to 10% smaller and in high northern latitudes about 2% smaller compared to the baseline run for the period between 2040 and 2050.

[60] Zonal and annual column ozone values do not allow the quantification of seasonal polar ozone depletion. In summer, the stratospheric circulation is weak and little ozone is transported to high latitudes. In addition, as in middle and low latitudes, ozone destroying cycles, mainly the NO_x cycle, result in decreasing ozone mixing ratios in the middle stratosphere. During fall and winter, meridional transport intensifies, with stronger downwelling in high latitudes, more pronounced in the NH. The ozone column increases until it reaches its maximum in spring, March/April in the Arctic and August/September in the Antarctic. Further, with decreasing sunlight ozone depleting cycles slow down. During late winter and spring, polar ozone chemistry is strongly disturbed owing to significant halogen activation and the resulting ozone depletion.

[61] To understand the influence of geoengineering in high polar latitudes, the annual evolution of monthly averaged column ozone values poleward of 70°S and 70°N equivalent latitudes is discussed (Figures 12b and 12c). Increasing heterogeneous reactions in the geoengineering run and changes in the stratospheric circulation and temperatures impact the column ozone in high latitudes, depending on season and hemisphere. For Antarctica, a significant difference between the geoengineering and baseline runs occurs between October and December, reaching 15%. Over the rest of the year, 5–10% smaller column ozone values were simulated in the geoengineering case. Column ozone values for the baseline run in 2040–2050 are above 250 DU and therefore indicate a recovery to 1980 values, which is ~20 years earlier than estimated by *Newman et al.* [2006], who based their results on the evolution of the effective equivalent stratospheric chlorine. WACCM underestimates the stratospheric Age of Air (AOA) owing to a too strong mean meridional circulation [see *Eyring et al.*, 2006]. The resulting overestimation of ozone transported in spring toward high latitudes is likely one reason for the underestimation of the recovery of polar ozone. In the geoengineering case, column ozone values are lower in October (222 DU ± 20 DU) compared to the baseline run. Therefore, geoengineering would significantly delay the recovery of ozone in high latitudes. This is analyzed further in section 6.

[62] In the Arctic, column ozone values increase significantly between 2010–2020 and 2040–2050 during winter and spring. In the geoengineering case, column ozone values in 2040–2050 between January and March are up to 4% smaller in the baseline run. However, as shown below, changes for the NH are underestimated by WACCM3 and could be significantly larger. The impact of geoengineering in the polar vortex is discussed below in section 6.

6. Changes in Polar Vortex Dynamics and Chemistry

6.1. Temperatures and Strength of the Polar Vortex

[63] The strength and location of the polar vortex can be quantified by using the gradient of modified potential vorticity (PV) times wind velocity with respect to equivalent latitude [e.g., *Bodeker et al.*, 2002; *Tilmes et al.*, 2006b]. The maximum of this quantity describes the location of the polar vortex edge. The value is a measure of the strength of the transport barrier.

[64] In Figure 13, we compare the strength and location of the polar vortex in the Arctic and Antarctica, as derived in *Tilmes et al.* [2006b], for the two simulations (averaged for all years between 2020 and 2050) with U.K. Meteorological Office analyses for 1992–2002. *Tilmes et al.* [2007] have shown that if running WACCM3 with a horizontal resolution of 4° × 5° the sharp polar vortex edge and a homogeneous vortex core (as seen in meteorological analyses) cannot be simulated in either the Arctic or Antarctica. However, these vortex characteristics improve significantly in a simulation run at 1.9° × 2.5° horizontal resolution for present-day conditions (the same as used in this study).

[65] Nevertheless, shortcomings are still present. The edge of the Antarctic polar vortex, defined as the location of the maximum PV gradient times the wind velocity, is 2–3° wider in both simulations than in the observations. The size of the homogeneous center of the vortex (between 90°S and 70°S), where the PV gradient times wind velocity is small, agrees very well with observations. The vortex in both model simulations is stronger before October and weaker during October compared to observations. Both simulations show a very similar vortex shape. In November, when the vortex becomes weaker, the transport barrier in the geoengineering run is stronger, because of the larger temperature gradient between middle and high latitudes [e.g., *Stenchikov et al.*, 2002].

[66] The polar transport barrier in both model simulations in the Arctic is located 2–5° farther poleward than in the observations. The wider maximum of the PV gradient times wind velocity results in a smaller homogeneous center of the vortex. The strength of the simulated Arctic transport barrier is in good agreement with observations in March. In February, the simulated transport barrier is weaker and in April it is stronger than observed. These results agree with the temperature evolution in the period of the vortex, which are warmer in the beginning of the Arctic winter and colder in spring compared to observations (not shown).

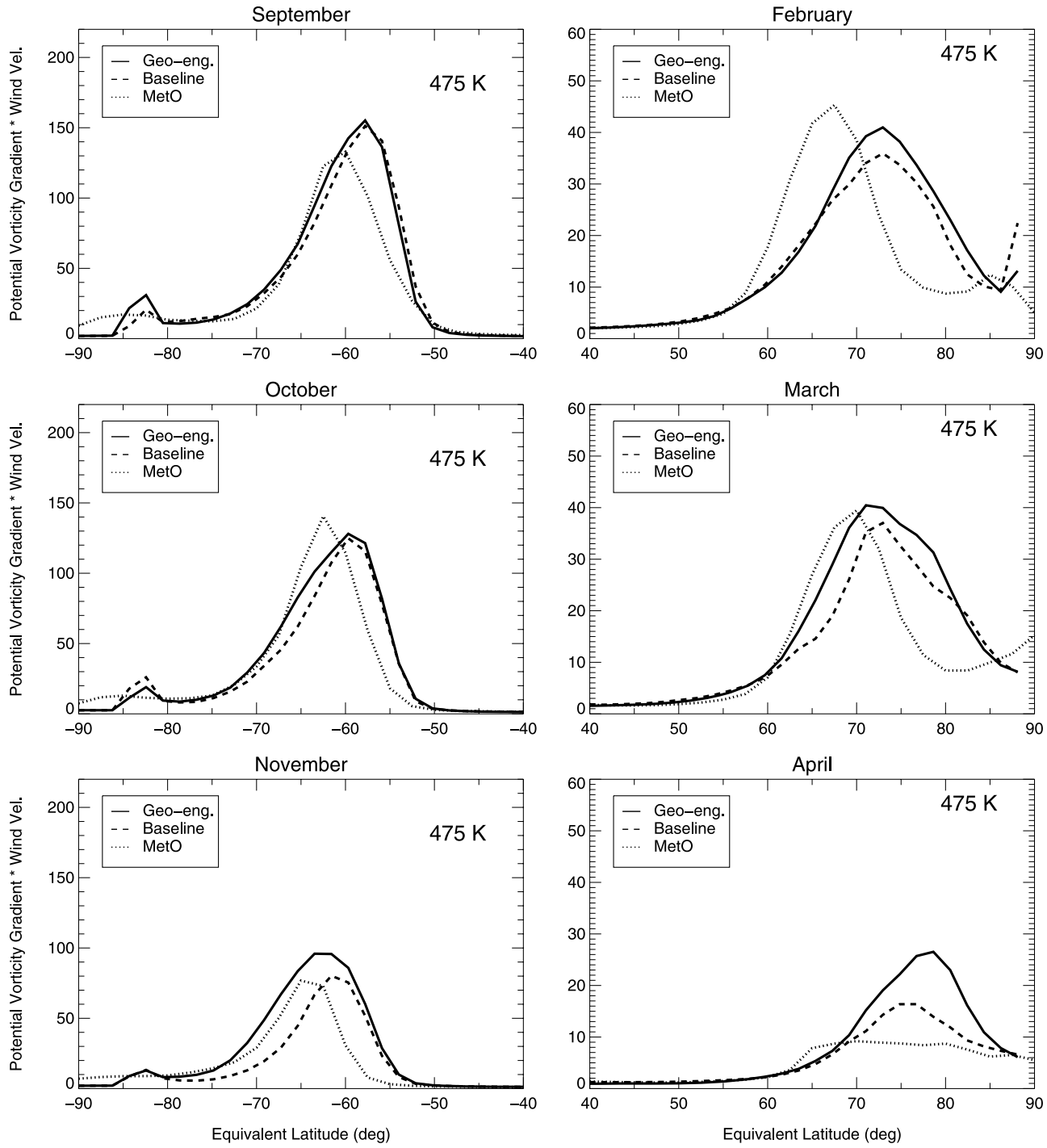

Figure 13. Gradient of modified potential vorticity (PV) times wind velocity with respect to equivalent latitude in different months at 475 K potential temperature. The baseline simulation (averaged between 2020 and 2050) is denoted by dashed lines; the geoengineered aerosol simulation (averaged between 2020 and 2050) is shown as solid lines; and the U.K. Meteorological Office analysis for 1992–2005 is indicated by dotted lines. (left) Southern Hemisphere and (right) Northern Hemisphere.

[67] For the Arctic, the location and width of the polar transport barrier cannot be reproduced in the WACCM3 model for present-day conditions (not shown), which are similar to the baseline run in 2020–2050. Nevertheless, between February and April, the geoengineering model run shows a stronger transport barrier compared to the baseline model run, especially in April. For both hemispheres, the polar vortex is stronger at the end of the winter in the geoengineered aerosol run and persists for a longer time. The stronger transport barrier of the polar vortex correlates with colder vortex temperatures for the geoengineering run (see Figure 14).

[68] In addition to the halogen abundance in the stratosphere, the evolution of chemical ozone depletion in the

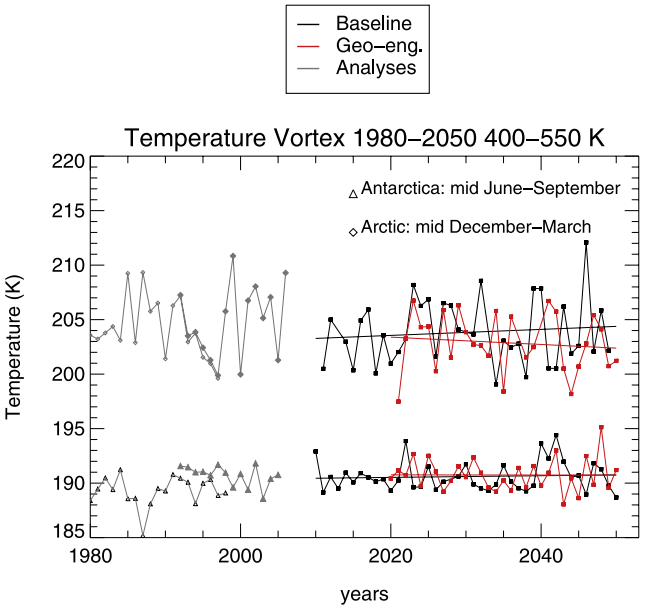

Figure 14. Averaged vortex temperatures between mid-December and the end of March for the Arctic and between mid-June and September for Antarctica in the baseline run (black line), the geoengineering run (red line), U.K. Meteorological Office analyses (grey and solid symbols) and European Center reanalyses (ERA40) (grey and open symbols) adopted from *Tilmes et al.* [2007].

polar region depends on the temperature evolution in the polar vortex. An analysis of observations in the past has been used to estimate the increase of chemical ozone depletion with changing climate, based on the assumption that polar vortex temperatures for cold Arctic winters decrease with changing climate conditions [*Knudsen et al.*, 2004; *Rex et al.*, 2006]. Here, a significant decrease of the temperatures in cold Arctic winters with changing climate conditions was not simulated, see below.

[69] In Figure 14, we compare vortex average temperatures between 400 and 550 K potential temperature for the Arctic and Antarctica for the two model simulations. In the Arctic vortex, even though temperatures in both model simulations are not significantly different, the geoengineering run (Figure 14, red lines) indicates a decrease in temperature of 1 K between 2020 and 2050, whereas vortex temperatures in the baseline run increase by 1 K between 2010 and 2050, with a rather low significance. Accordingly, in 2050, the vortex of the geoengineering simulation is 2 K colder compared to the baseline run. Baseline results show a similar annual temperature variability as derived from meteorological analysis between 1980 and 2005 (grey lines). Coldest winters in the geoengineering model run show up to 2 K lower temperatures compared to the baseline model run and meteorological analyses in the NH polar vortex. In contrast, similar temperature changes due to geoengineering in high northern latitudes could not be found considering annual mean zonally averaged values, as shown in Figure 3, because of the frequent displacement of the NH vortex in lower latitudes.

[70] Lower temperatures and a stronger polar vortex in the geoengineering run, which results in a longer period with cold temperatures, favor chemical ozone depletion compared to the baseline run. Further, strongly enhanced SAD reduce the threshold temperature for chlorine activation and ozone catalytic cycles can be much more effective for the geoengineering run.

[71] For Antarctica, temperatures in the baseline and geoengineering runs are the same on average and have no significant temperature trend. Increasing temperatures below 30 km in the annual average in Figure 3 occur therefore mainly in summer and fall in both hemispheres. The stronger simulated Antarctic vortex in November and cooler temperatures in the vortex between October and January in the geoengineering case compared to the baseline run are not included in the vortex average in Figure 14. As for the Arctic, enhanced SAD values change in the activation temperature and result in a larger potential for ozone depletion, as discussed below.

6.2. Impact of Geoengineered Aerosol on Chemical Ozone Depletion

[72] Chemical ozone depletion in WACCM3 is calculated using the tracer-tracer correlation technique. A detailed description of the technique and its application to the WACCM3 REF1 model simulation was performed by *Tilmes et al.* [2007]. *Tilmes et al.* [2007] showed that WACCM3 underestimates Arctic chemical ozone depletion for present-day conditions using a coarser ($4^\circ \times 5^\circ$) horizontal model resolution than in the present runs. For Antarctica, on the other hand, chemical ozone depletion comparable to that observed could be reproduced for the polar vortex core. Using a higher horizontal resolution, the simulation of Arctic chemical ozone loss has improved, and losses up to 50 DU were simulated for the coldest winter in the past (Figure 15, top, open diamonds). However, the improvements are not sufficient to simulate reliably the ozone depletion in the Arctic polar stratosphere, and chemical ozone depletion is on average less than half as large as derived from observations (Figure 15, top). Even though vortex average temperatures for the baseline run are comparable to results derived using meteorological analyses, the Arctic polar vortex is too small and the width of the transport barrier is too wide, as discussed above. An underestimation of chemical ozone depletion is therefore expected because (1) the homogeneous area of the vortex is too small and is not illuminated early enough, so the start of chemical ozone depletion is delayed; (2) temperatures are too warm at the beginning of the winter to build up sufficient amounts of the active chlorine; and (3) there is possibly not enough total bromine in the simulation to produce sufficient ozone depletion in the Arctic.

[73] For the baseline model run, chemical ozone depletion in the Arctic reaches only 50 DU for the coldest winter, in 2018. In the period 2040–2050, even with decreasing halogen amounts, chemical ozone depletion still reaches nearly 40 DU. For the geoengineering run, depletion reaches 94 DU for the coldest winter, 2021, and more than 70 DU in the last decade of the simulation. These results agree well with observational estimates for comparable temperature conditions, namely moderately cold winters, discussed by *Tilmes et al.* [2008]. The 1–2 times increase in chemical ozone depletion results from the combination of colder

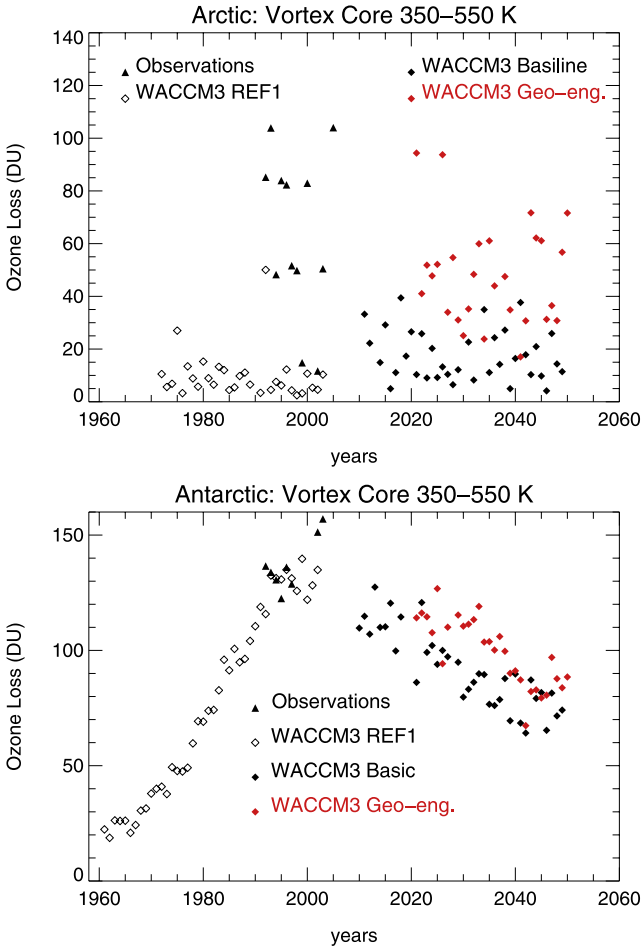

Figure 15. Accumulated chemical ozone loss between the early winter reference function and (top) in the beginning of April for the Arctic vortex core and (bottom) in mid-October for the Antarctic vortex core, between 350 and 550 K. Between 1970 and 2003, WACCM3 results of the REF1 simulation are shown; between 1992 and 2004, HALOE accumulated chemical ozone are shown as black triangles [*Tilmes et al.*, 2006a]; between 2010 and 2050, WACCM3 baseline results are shown as black diamonds and geoengineering results are shown as red diamonds. Future results are also shown by *Rasch et al.* [2008a].

Arctic winters, strong polar transport barrier, and the enhanced heterogeneous reaction in the geoengineering run.

[74] For Antarctica, chemical ozone depletion in the polar vortex shows less variability and was saturated between 1992 and 2004 on the basis of observations [*Tilmes et al.*, 2006a]. Most of the ozone in the lower stratosphere was depleted and increasing chlorine activation does not significantly impact the amount of ozone depletion after 1990, as derived earlier using the WACCM3 REF1 simulation. The baseline model simulation shows slowly decreasing ozone loss between 2010 and 2050, due to the decreasing halogen content in the stratosphere. By 2050, ozone depletion of 60–80 DU still occurs each year in the model. For the geoengineered aerosol run, Antarctic ozone depletion is in general 40–50 DU larger than in the baseline run and does not begin to decrease before 2030. In the geoengineering case, ozone depletion in 2040–2050 reaches values comparable to 2015–2025 in the baseline case. Therefore, the recovery of ozone depletion is delayed by about 30 years in this model study. By 2050, chemical ozone depletion still shows values above 100 DU for some Antarctic winters in the geoengineering run. In comparison to other studies [*Tilmes et al.*, 2008; *Newman et al.*, 2007], ozone depletion in the baseline and the geoengineering run is saturated for ≈20 years before it starts decreasing. Therefore, the delay of the ozone hole recovery is possibly underestimated.

7. Summary and Conclusions

[75] A fully interactive chemistry climate model, WACCM3, was used to simulate the impact of a hypothetical geoengineering approach to counteract tropospheric greenhouse warming between 2020–2050. A constant, enhanced distribution of volcanic-sized aerosols was prescribed in the lower stratosphere, and used in a transient model run with changing greenhouse gases and stratospheric halogen content. We do not discuss practical implementations of how to produce a specific aerosol distribution, and refer to *Rasch et al.* [2008a] for details. The purpose of this study is instead to explore the impact and side effects of the hypothetical injection of a fixed amount of sulfur on the climate system and on stratospheric processes. For this reason, and because our simulation does not include a detailed microphysical model for the aerosols, we have adopted the most reasonable aerosol size distribution, with effective radii corresponding to volcanic-sized particles. We find that the enhancement of the stratospheric aerosol content resulting from the injection of 2 Tg S per year of volcanic-sized particles is necessary to counteract global warming by around 2050.

[76] The injection of a constant amount of sulfur in the stratosphere, as considered here, results in a constant offset of temperatures in the tropics at different altitudes after an adjustment time in the troposphere of approximately 5 years. The strongest cooling in the tropics of about 2 K occurs at around 11 km in the geoengineering run compared to the baseline run. A positive tropospheric temperature trend as a result of increasing greenhouse gases between 2020 and 2050 is present in both simulations, since the geoengineered aerosol content does not change with time. The initial cooling achieved owing to geoengineering is overwhelmed by increasing greenhouse gases after about four decades. Therefore, the injection of 2 Tg S/a sulfur into the stratosphere would delay global warming by some 40 years, assuming a volcanic-sized aerosol size distribution.

[77] The surface temperature response to geoengineering shows the expected cooling. Enhanced SAD result in surface temperatures in 2040–2050 that are ∼0.5° below present-day conditions, and show significant local changes of between +1 and −3 K. Surface cooling in the polar regions in the geoengineering case prevents a decrease in the Arctic sea-ice fraction, which is otherwise calculated to diminish by 15% in the baseline run owing to increasing, uncompensated greenhouse warming. Changes in the precipitation patterns between 2010–2020 and 2040–2050 are not very significant in either model simulation. However, the precipitation was found to decrease by 0.5–0.8 mm per day in the tropics in the geoengineering case.

[78] The annual averaged decrease in surface temperatures produced by geoengineered aerosols was shown to be about 1 K larger in a run with NCAR's Community Atmosphere Model (CAM) than in WACCM3. Even though the model setup in the simulations with CAM and WACCM3 was not the same, strong differences at high latitudes, particularly in winter, indicate the influence of stratospheric processes in the geoengineering model simulation using WACCM3.

[79] In the case of geoengineering, the strongly enhanced SAD in the lower stratosphere results in an increase of heterogeneous reactions. Around 25–27 km, the ozone-destroying NO_x catalytic cycle slows down significantly in the tropics and midlatitudes. This leads to an increase in ozone which in turn causes O_x production between 22 and 26 km to decrease owing to a decrease in UV radiation reaching this region. On the other hand, other ozone destroying cycles increase, especially the HO_x cycle in the tropics and midlatitudes, and the ClO_x cycle in high polar regions of the SH between 15 and 20 km. Below 28 km, advection influences ozone in the tropics and high latitudes. In the geoengineering case, changes in advection result in a significant increase of ozone between 15 and 22 km in the tropics.

[80] On a global scale, increasing greenhouse gases and a decreasing halogen content are expected to result in a slight increase of the ozone column in low latitudes and midlatitudes and a significant increase in the SH in 2040–2050 compared to 2010–2020. The use of geoengineered aerosols to cool the troposphere results in a slight increase of column ozone at latitudes 10°N–30°N and 10°S–30°S compared to the baseline run. At high latitudes, column ozone is reduced up to 10% in the geoengineering case, with seasonal changes being most pronounced during spring. Compared to the baseline simulation, the use of geoengineered sulfate aerosols to counteract global warming would delay the effects of decreasing halogen compounds in the stratosphere following from the Montreal Protocol and its amendments and adjustments by 20–30 years, although ozone depletion is not calculated to become worse compared to present-day baseline conditions. The impact of geoengineered aerosols on the column ozone in the NH cannot be precisely quantified, owing to a significant underestimation of ozone depletion in the Arctic polar vortex in the model. Even so, we do not anticipate catastrophic changes in stratospheric chemistry and dynamics under the geoengineering approach considered here, which effectively cools the troposphere.

[81] Owing to large interannual temperature variations of the Arctic polar vortex, the impact of geoengineering in single years is much more pronounced. A stronger, longer-lived polar transport barrier results in colder Arctic winters in the geoengineering run compared to the baseline run. In addition, enhanced heterogeneous reactions allow for intensified chlorine activation in high polar regions. Even though WACCM3 underestimates Arctic chemical ozone depletion in comparison to observations, the simulation shows an onefold to twofold increase in ozone depletion in the case of geoengineering in the NH, in agreement with observational estimates by *Tilmes et al.* [2008]. For 2040–2050 conditions, Arctic ozone depletion might be larger than seen hitherto for cold Arctic winters. This may not change the dynamics of the stratosphere drastically, but might have an impact on tropospheric conditions. The up to 10% increase in UV radiation observed in middle and high latitudes between the 1980s and 1990s [*Lee-Taylor and Madronich*, 2007] would probably worsen in the future, with dangerous effects for the ecosystem. Additional model studies are desirable to simulate the impact of a more precise calculation of NH ozone depletion.

[82] Aside from the potential for serious ozone deficits in high northern latitudes in winter and spring, and possible large local changes in temperature and precipitation, large uncertainties remain about how geoengineering would influence the climate system and the biosphere, as noted by *Rasch et al.* [2008a]. Therefore, much more research is necessary to resolve many outstanding issues. Technical solutions and costs need to be investigated in greater detail. It should also be borne in mind that injection of sulfur into the tropical stratosphere above ~25 km is probably necessary for this approach to achieve the required aerosol distribution across the entire planet. Issues surrounding the timing of aerosol deployment, as well as the amount of desired cooling, and its effectiveness in the context of, say, incipient rapid disintegration of the Greenland ice sheets need to be studied. Finally, considering the legal, political and ethical complications of any possible emergency deployment of this or other geoengineering schemes, it is clear that such approaches are tools of last resort. The focus of efforts to avoid undesirable climate impacts must continue to be the substantial and rapid reduction of greenhouse gas emissions.

[83] **Acknowledgments.** We gratefully acknowledge the members of the HALOE team at NASA/Langley Research Center for their work in producing and making available the HALOE data set. Thanks are also owed to the U.K. Meteorological Office and the European Center for Medium-range Weather Forecasts for providing meteorological analyses. Further, we thank the WACCM team, especially Francis Vitt, Stacy Walters, and Fabrizio Sassi, for assistance with regard to the WACCM3 model setup and analysis tools. We also thank Michael Mills and Brian Toon for helpful discussions on microphysical processes in connection with stratospheric sulfur injection. Finally, we are grateful to Steven Massie and John Orlando for their review of the original manuscript. The National Center for Atmospheric Research is operated by the University Corporation for Atmospheric Research under sponsorship of the National Science Foundation.

References

Bodeker, G. E., H. Struthers, and B. J. Connor (2002), Dynamical containment of Antarctic ozone depletion, *Geophys. Res. Lett.*, *29*(7), 1098, doi:10.1029/2001GL014206.

Brasseur, G., and S. Solomon (2005), *Aeronomy of the Middle Atmosphere: Chemistry and Physics of the Stratosphere and Mesosphere*, 3rd ed., Springer, Heidelberg, Germany.

Budyko, M. I. (1977), *Climatic Changes*, translated from Russian by R. Zolina, AGU, Washington, D. C.

Cai, M. (2005), Dynamical amplification of polar warming, *Geophys. Res. Lett.*, *32*, L22710, doi:10.1029/2005GL024481.

Cicerone, R. J. (2006), Geoengineering: Encouraging research and overseeing implementaion, *Clim. Change*, *77*, 221–226.

Collins, W. J., et al. (2006), The formulation and atmospheric simulation of the community atmosphere model (CAM3), *J. Clim.*, *19*, 2144–2161.

Considine, D. B., A. R. Douglass, D. E. Kinnison, P. S. Connell, and D. A. Rotman (2000), A polar stratospheric cloud parameterization for the three-dimensional model of the global modeling initiative and its response to stratospheric aircraft emissions, *J. Geophys. Res.*, *105*, 3955–3975.

Crutzen, P. J. (2006), Albedo enhancements by stratospheric sulfur injections: A contribution to resolve a policy dilemma? An editorial essay, *Clim. Change*, *77*, 211–219.

Drdla, K. (2005), Temperature thresholds for polar stratospheric ozone loss, *Eos Trans. AGU*, *86*(52), Fall Meet. Suppl., Abstract A31D-03.

Eyring, V., et al. (2005), A strategy for process-oriented validation of coupled chemistry-climate models, *Bull. Am. Meteorol. Soc.*, *86*(8), 1117–1133.

Eyring, V., et al. (2006), Assessment of temperature, trace species and ozone in chemistry-climate simulations of the recent past, *J. Geophys. Res.*, *111*, D22308, doi:10.1029/2006JD007327.

Fahey, D. W., et al. (1993), In situ measurements constraining the role of sulphate aerosols in mid-latitude ozone depletion, *Nature*, *363*, 509–514.

Garcia, R. R., and W. J. Randel (2008), Acceleration of Brewer-Dobson circulation due to increase in greenhouse gases, *J. Atmos. Sci.*, *65*, 2731–2739.

Garcia, R. R., D. R. Marsh, D. E. Kinnison, B. A. Boville, and F. Sassi (2007), Simulation of secular trends in the middle atmosphere, *J. Geophys. Res.*, *112*, D09301, doi:10.1029/2006JD007485.

Grooß, J.-U., R. Müller, G. Becker, D. S. McKenna, and P. J. Crutzen (1999), The upper stratospheric ozone budget: An update of calculations based on HALOE data, *J. Atmos. Chem.*, *34*, 171–183.

Intergovernmental Panel on Climate Change (2007), *Climate Change 2007: The Physical Science Basis*, *Contribution of Working Group I to the Fourth Assessment Report of the Intergovernmental Panel on Climate Change*, Cambridge Univ. Press, Cambridge, U. K.

Kiehl, J. T., B. A. Boville, and B. P. Briegleb (1988), Response of a general circulation model to a prescribed Antarctic ozone hole, *Nature*, *332*, 501–504.

Kinnison, D. E., et al. (2007), Sensitivity of chemical tracers to meteorological parameters in the MOZART-3 chemical transport model, *J. Geophys. Res.*, *112*, D20302, doi:10.1029/2006JD007879.

Knudsen, B. M., N. R. P. Harris, S. B. Andersen, B. Christiansen, N. Larsen, M. Rex, and B. Naujokat (2004), Extrapolating future Arctic ozone losses, *Atmos. Chem. Phys.*, *4*, 1849–1856.

Lee-Taylor, J., and S. Madronich (2007), Climatology of UV-A, UV-B, and erythemal radiation at the Earth's surface, 1979–2000, *NCAR Tech. Note TN-474+STR*, 52 pp., Natl. Cent. for Atmos. Res., Boulder, Colo.

Marsh, D., R. R. Garcia, D. E. Kinnison, B. A. Bouville, F. Sassi, S. C. Solomon, and K. Matthes (2007), Modeling the whole atmosphere response to solar cycle changes in radiative and geomagnetic forcing, *J. Geophys. Res.*, *112*, D23306, doi:10.1029/2006JD008306.

Metz, B., et al. (Eds.) (2005), *Special Report on Safeguarding the Ozone Layer and the Global Climate System: Issues Related to Hydrofluorocarbons and Perfluorocarbons*, Cambridge Univ. Press, Cambridge, U. K.

Mills, M. J. (1996), Stratospheric sulfate aerosol: A microphysical model, Ph.D. thesis, Univ. of Colo., Boulder.

Newman, P. A., E. R. Nash, S. R. Kawa, S. A. Montzka, and S. M. Schauffler (2006), When will the Antarctic ozone hole recover?, *Geophys. Res. Lett.*, *33*, L12814, doi:10.1029/2005GL025232.

Newman, P. A., J. S. Daniel, D. W. Waugh, and E. R. Nash (2007), A new formulation of equivalent effective stratospheric chlorine (EESC), *Atmos. Chem. Phys.*, *7*, 4537–4552.

Perlwitz, J., S. Pawson, R. Fogt, J. Nielsen, and W. Neff (2008), Impact of stratospheric ozone hole recovery on Antarctic climate, *Geophys. Res. Lett.*, *35*, L08714, doi:10.1029/2008GL033317.

Randel, W. J., et al. (2009), An update of observed stratospheric temperature trend, *J. Geophys. Res.*, *114*, D02107, doi:10.1029/2008JD010421.

Rasch, P. J., S. Tilmes, R. P. Turco, A. Robock, L. Oman, and C.-C. Chen (2008a), An overview of geoengineering of climate using stratospheric sulphate aerosols, *Proc. R. Soc., Ser. A*, *366*, 4007–4037.

Rasch, R. J., C. P. J., and D. B. Coleman (2008b), Exploring the geoengineering of climate using stratospheric sulfate aerosols: The role of particle size, *Geophys. Res. Lett.*, *35*, L02809, doi:10.1029/2007GL032179.

Rex, M., et al. (2006), Arctic winter 2005: Implications for stratospheric ozone loss and climate change, *Geophys. Res. Lett.*, *33*, L23808, doi:10.1029/2006GL026731.

Robock, A. (2000), Volcanic eruptions and climate, *Rev. Geophys.*, *38*, 191–219.

Robock, A., L. Oman, and G. Stenchikov (2008), Regional climate response to geoengineering with tropical and arctic SO_2 injection, *J. Geophys. Res.*, *113*, D16101, doi:10.1029/2008JD010050.

Russell, P. B., et al. (1996), Global to microscale evolution of the Pinatubo volcanic aerosol derived from diverse measurements and analyses, *J. Geophys. Res.*, *101*, 18,745–18,763.

Sassi, F., B. A. Boville, D. Kinnison, and R. Garcia (2005), The effects of interactive ozone chemistry on simulations of the middle atmosphere, *Geophys. Res. Lett.*, *32*, L07811, doi:10.1029/2004GL022131.

Seinfeld, J. H., and S. N. Pandis (1998), *Atmospheric Chemistry and Physics*, John Wiley, Hoboken, N. J.

Solomon, S. (1999), Stratospheric ozone depletion: A review of concepts and history, *Rev. Geophys.*, *37*, 275–316.

Solomon, S., R. Portmann, R. R. Garcia, L. Thomason, L. R. Poole, and M. P. McCormick (1996), The role of aerosol variations in anthropogenic ozone depletion at northern midlatitudes, *J. Geophys. Res.*, *101*, 6713–6727.

Son, S.-W., et al. (2008), The impact of stratospheric ozone recovery on the Southern Hemisphere westerly jet, *Science*, *320*, 1486–1489.

Stenchikov, G. L., A. Robock, V. Ramaswamy, M. D. Schwarzkopf, K. Hamilton, and S. Ramachandran (2002), Oscillation response to the 1991 Mount Pinatubo eruption: Effects of volcanic aerosols and ozone depetion, *J. Geophys. Res.*, *107*(D24), 4803, doi:10.1029/2002JD002090.

Tabazadeh, A., K. Drdla, M. R. Schoeberl, P. Hamill, and O. B. Toon (2002), Arctic "ozone hole" in a cold volcanic stratosphere, *Proc. Natl. Acad. Sci. U. S. A.*, *99*(5), 2609–2612.

Thomason, L., and T. Peter (Eds.) (2006), SPARC assessment of Stratospheric aerosol properties, *WMO/TD1295*, World Meteorol. Org., Geneva, Switzerland.

Thomason, L. W., L. R. Poole, and T. Deshler (1997), A global climatoloy of stratospheric aerosol surface area density deduced from Stratospheric Aerosol and Gas Experiment II measurements: 1984–1994, *J. Geophys. Res.*, *102*, 8967–8976.

Thompson, D., and S. Solomon (2002), Interpretation of recent Southern Hemisphere climate change, *Science*, *296*, 895–899.

Thompson, D. W. J., M. P. Baldwin, and S. Solomon (2005), Stratosphere-troposphere coupling in the Southern Hemisphere, *J. Atmos. Sci.*, *62*, 708–715.

Tilmes, S., R. Müller, A. Engel, M. Rex, and J. Russel III (2006a), Chemical ozone loss in the Arctic and Antarctic stratosphere between 1992 and 2005, *Geophys. Res. Lett.*, *33*, L20812, doi:10.1029/2006GL026925.

Tilmes, S., R. Müller, J.-U. Grooß, H. Nakajima, and Y. Sasano (2006b), Development of tracer relations and chemical ozone loss during the setup phase of the polar vortex, *J. Geophys. Res.*, *111*, D24S90, doi:10.1029/2005JD006726.

Tilmes, S., D. Kinnisen, R. Müller, F. Sassi, D. Marsh, B. Boville, and R. Garcia (2007), Evaluation of heterogeneous processes in the polar lower stratosphere in the Whole Atmosphere Community Climate Model, *J. Geophys. Res.*, *112*, D24301, doi:10.1029/2006JD008334.

Tilmes, S., R. Müller, and R. J. Salawitch (2008), The sensitivity of polar ozone depletion to proposed geoengineering schemes, *Science*, *320*, 1201–1204.

Turco, R. P., P. Hamill, O. B. Toon, R. C. Whitten, and C. S. Kiang (1979), The NASA-Ames Research Center stratospheric aerosol model, I, Physical processes and mathematical analogs, *J. Atmos. Sci.*, *36*, 699–717.

United Nations Environment Programme and Environmental Effects Assessment Panel (2005), Environmental effects of ozone depletion and its interactions with climate change: Progress report, 2004, *Photochem. Photobiol. Sci.*, *4*(2), 177–184.

Wigley, T. M. (2006), A combined mitigation/geoengineering approach to climate stabilization, *Science*, *314*, 452–454.

Zhao, J., R. P. Turco, and O. B. Toon (1995), A model simulation of Pinatubo volcanic aerosols in the stratosphere, *J. Geophys. Res.*, *100*, 7315–7328.

R. R. Garcia, A. Gettelman, D. E. Kinnison, and S. Tilmes, Atmospheric Chemistry Division, National Center of Atmospheric Research, P.O. Box 3000, Boulder, CO 80307-3000, USA. (tilmes@ucar.edu)

P. J. Rasch, Pacific Northwest National Laboratory, 902 Battelle Boulevard, P.O. Box 999, MSIN K9-34, Richland, WA 99352, USA.